Department of Electrical Engineering and Automation

Identification and Speed Control Design of Resonating Mechanical Systems in Electric Drives

Seppo Saarakkala

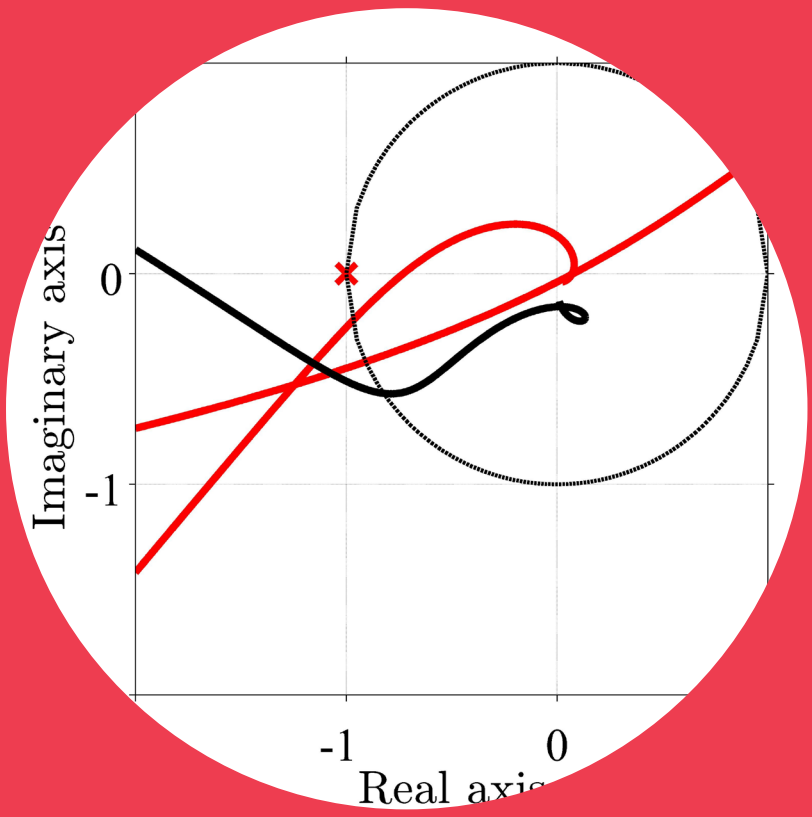

Aalto University

DOCTORAL DISSERTATIONS

Aalto University publication series
DOCTORAL DISSERTATIONS 126/2014

Identification and Speed Control Design of Resonating Mechanical Systems in Electric Drives

Seppo Saarakkala

A doctoral dissertation completed for the degree of Doctor of Science (Technology) to be defended, with the permission of the Aalto University School of Electrical Engineering, at a public examination held at the lecture hall S1 of the school on 3 October 2014 at 12.

Aalto University
School of Electrical Engineering
Department of Electrical Engineering and Automation
Electric drives

Supervising professors
Prof. Jorma Luomi
Prof. Marko Hinkkanen

Thesis advisor
Prof. Marko Hinkkanen

Preliminary examiners
Prof. Mario Pacas, University of Siegen, Germany
Prof. Teresa Orlowska-Kowalska, Wroclaw University of Technology, Poland

Opponent
Dr. Luca Peretti, ABB AB, Corporate Research, Sweden

Aalto University publication series
DOCTORAL DISSERTATIONS 126/2014

ISBN 978-952-60-5826-9
ISBN 978-952-60-5827-6 (pdf)
ISSN-L 1799-4934
ISSN 1799-4934 (printed)
ISSN 1799-4942 (pdf)
http://urn.fi/URN:ISBN:978-952-60-5827-6

Unigrafia Oy
Helsinki 2014

Finland

441 697
Printed matter

Aalto University

Abstract

Aalto University, P.O. Box 11000, FI-00076 Aalto www.aalto.fi

Author
Seppo Saarakkala

Name of the doctoral dissertation
Identification and Speed Control Design of Resonating Mechanical Systems in Electric Drives

Publisher School of Electrical Engineering

Unit Department of Electrical Engineering and Automation

Series Aalto University publication series DOCTORAL DISSERTATIONS 126/2014

Field of research Electric drives

Manuscript submitted 22 March 2014 **Date of the defence** 3 October 2014

Permission to publish granted (date) 24 June 2014 **Language** English

☐ **Monograph** ☒ **Article dissertation (summary + original articles)**

Abstract

Ac electrical machines supplied with a frequency converter have been increasingly selected for torque actuators in modern motion control applications. These applications often contain several moving or rotating masses connected together with mechanical transmission components. This configuration results in mechanical resonances and, if the speed-feedback loop is delayed, instability can even occur. To overcome the resonance problems, several speed control methods and different tuning approaches have been proposed: They range from the gain decreasing of a simple proportional integral (PI) controller to the use of complex nonlinear controllers. This dissertation provides methods to analytically tune the speed controller of electrical drives. The tuning rules are given for both a rigid single-mass system and a resonating two-mass system. The speed controller is designed to give both the robust regulation performance as well as accurate reference tracking. The controller gains are always parametrized in the parameters of the mechanical system and in some design specifications, which results in the possibility of applying gain scheduling if required. The dissertation demonstrates on an experimental level that an effective and robust classical speed controller can be designed for both the rigid single-mass system as well as the resonating two-mass system. However, the controlled mechanical-system model must be known and the controller must be tuned using the known model. Finding a suitable mechanical model and its parameters may sometimes be problematic. Not all of parameters are always available or else the datasheet values may not be accurate. To overcome the problems of finding the mechanical parameters, this dissertation provides methods to identify the mechanical load and its parameters. The identification can be done both in the open-loop and closed-loop operations and it is based on using discrete-time polynomial models instead of frequency-domain methods. The experiments established that the polynomial-model based, discrete-time method is a better choice, than the frequency-response-based method. This is mainly because of the absence of the time domain to the frequency domain conversion, which adds an additional computational burden and numerical inaccuracy to the identification method. The experiments further demonstrate that the proposed identification method can be successfully applied both in the open-loop and in the closed-loop configurations.

Keywords identification, motion control, parameter estimation, resonating system, speed control

ISBN (printed) 978-952-60-5826-9 **ISBN (pdf)** 978-952-60-5827-6

ISSN-L 1799-4934 **ISSN (printed)** 1799-4934 **ISSN (pdf)** 1799-4942

Location of publisher Helsinki **Location of printing** Helsinki **Year** 2014

Pages 174 **urn** http://urn.fi/URN:ISBN:978-952-60-5827-6

A! Aalto-yliopisto

Tiivistelmä

Aalto-yliopisto, PL 11000, 00076 Aalto www.aalto.fi

Tekijä
Seppo Saarakkala

Väitöskirjan nimi
Sähkökäytön joustavan mekaniikan identifiointi ja nopeussäädön suunnittelu

Julkaisija Sähkötekniikan korkeakoulu

Yksikkö Sähkötekniikan ja automaation laitos

Sarja Aalto University publication series DOCTORAL DISSERTATIONS 126/2014

Tutkimusala Sähkökäytöt

Käsikirjoituksen pvm 22.03.2014 **Väitöspäivä** 03.10.2014

Julkaisuluvan myöntämispäivä 24.06.2014 **Kieli** Englanti

☐ **Monografia** ☒ **Yhdistelmäväitöskirja (yhteenveto-osa + erillisartikkelit)**

Tiivistelmä

Taajuusmuuttajalla syötetty vaihtosähkömoottori valitaan yhä useammin nykyaikaisten liikkeenohjaussovellusten toimilaitteeksi. Liikkeenohjaussovelluksissa on yleensä useita liikkuvia tai pyöriviä massoja, jotka kytketään toisiinsa käyttäen mekaanisia välityksiä. Mekaanisesti toisiinsa kytketyt massat aiheuttavat järjestelmään resonanssi-ilmiöitä ja jos nopeustakaisinkytkentä on viiveellinen, järjestelmä voi jopa ajautua epästabiiliin tilaan. Useita erilaisia nopeussäätörakenteita ja säätäjien viritystapoja on ehdotettu resonanssi-ilmiön aiheuttamien ongelmien välttämiseksi. Yksinkertaisimmillaan voidaan klassisen PI-säätäjän vahvistuksia pienentää. Vaihtoehtoisesti voidaan soveltaa monimutkaisia epälineaarisia säädinrakenteita. Tässä työssä ehdotetaan analyyttisiä menetelmiä sähkökäytön nopeussäätimen suunnitteluun. Säätimen viritysohjeet annetaan sekä jäykälle yhden massan järjestelmälle että värähtelevälle kahden massan järjestelmälle. Nopeussäädin suunnitellaan siten, että saavutetaan hyvä kuormahäiriön sietokyky ja tarkka asetusarvon seuranta. Säätimen vahvistukset valitaan aina mekaanisten parametrien ja viritysehtojen funktiona. Tämä mahdollistaa tarvittaessa vahvistustaulukoinnin käytön. Tässä työssä osoitetaan kokeellisesti, että jäykälle yhden massan järjestelmälle ja värähtelevälle kahden massan järjestelmälle voidaan virittää suorituskykyinen ja robusti nopeussäädin käyttäen ainoastaan klassisen säätöteorian menetelmiä. Tämä edellyttää sitä, että säädettävä mekaaninen järjestelmä parametreineen tunnetaan kohtalaisella tarkkuudella ja nopeussäädin suunnitellaan käyttäen tunnettua järjestelmämallia. Mekaanisen järjestelmän parametrien määrittäminen ei ole välttämättä helppoa. Kaikkia tarvittavia parametreja ei ole aina saatavillla, tai parametriarvojen määrittäminen datalehtien avulla voi johtaa epätarkkoihin tuloksiin. Jotta parametriarvojen määrittämiseen liittyvät ongelmat voitaisiin välttää, tässä työssä esitetään menetelmä identifioida kuorman malli parametreineen. Identifiointi voidaan tehdä joko avoimessa järjestelmässä tai nopeustakaisinkytketyssä järjestelmässä. Ehdotettu identifiointimenetelmä perustuu diskreettiaikaisten polynomien käyttöön taajuusvastemenetelmien sijasta. Tässä työssä osoitetaan kokeellisesti, että diskreettiaikaisiin polynomeihin perustuva identifiointimenetelmä on taajuusvastemenetelmää parempi vaihtoehto. Tämä johtuu siitä, että polynomimalleja käytettäessä ei aikatasossa mitattuja signaaleja tarvitse muuntaa taajuustasoon. Tällöin vältytään sekä ylimääräiseltä laskennalta että muunnoksen epätarkkuudesta aiheutuvilta virheiltä.

Avainsanat identifiointi, liikkeenohjaus, nopeussäätö, parametrien estimointi, värähtelevä järjestelmä

ISBN (painettu) 978-952-60-5826-9 **ISBN (pdf)** 978-952-60-5827-6

ISSN-L 1799-4934 **ISSN (painettu)** 1799-4934 **ISSN (pdf)** 1799-4942

Julkaisupaikka Helsinki **Painopaikka** Helsinki **Vuosi** 2014

Sivumäärä 174 **urn** http://urn.fi/URN:ISBN:978-952-60-5827-6

Preface

The research work reported in this dissertation was carried out between July 2008 and December 2009 in Lappeenranta University of Technology (LUT) and between January 2010 and December 2013 in Aalto University School of Electrical Engineering in research projects funded by ABB Oy. I am obligated to be able to work in such well organized and interesting projects.

I would like to thank my supervisors and colleagues at LUT for introducing me the exiting academic world. I am grateful to Prof. Jorma Luomi for giving me the opportunity to join the electric drives group at the Aalto University and giving me instructions how to prepare publications. However, it is due to my dissertation supervisor and advisor Prof. Marko Hinkkanen, that this work is finally completed. Your contribution has been substantial, and I am deeply grateful for that. Furthermore, I would like to thank Dr. Markku Jokinen from ABB Oy for the fruitful cooperation throughout the whole dissertation work. The discussions with Mr. Matti Mustonen are also highly valued.

Because the preparation of this dissertation took a relatively long time, the list of people to be thanked for would easily grow to unbearable extent. Though, instead of individual thank-you's, I would like to express my sincerest gratitude, whether you are a colleague, a relative, or a friend, for tolerating my yapping about the ups and downs during the research work. Hopefully I can pay back something, when we celebrate the Karonkka party.

The additional financial support by Walter Ahlström Foundation, Emil Aaltonen Foundation, and The Research Foundation of Helsinki University of Technology is most gratefully acknowledged.

Helsinki, August 26, 2014,

Seppo Saarakkala

Contents

List of Publications

This thesis consists of an overview and of the following publications which are referred to in the text by their Roman numerals.

I Markku Jokinen, Seppo E. Saarakkala, Markku Niemelä, Riku Pöllänen, Juha Pyrhönen. Physical Drawbacks of Linear High Speed Tooth Belt Drives. In *International Symposium on Power Electronics, Electrical Drives, Automation and Motion (SPEEDAM)*, 6 p., Ischia, Italy, June 2008.

II Seppo E. Saarakkala, Antti Alahäivälä, Marko Hinkkanen, Jorma Luomi. Dynamic Emulation of Multi-Mass Mechanical Loads in Electric Drives. In *14th European Conference on Power Electronics and Applications (EPE)*, 10 p., Birmingham, United Kingdom, August-September 2011.

III Seppo E. Saarakkala, Tuomo Leppinen, Marko Hinkkanen, Jorma Luomi. Parameter Estimation of Two-Mass Mechanical Loads in Electric Drives. In *The 12th International Workshop on Advanced Motion Control (AMC)*, 6 p., Sarajevo, Bosnia Hertzegovina, March 2012.

IV Seppo E. Saarakkala, Marko Hinkkanen, Kai Zenger. Speed Control of Two-Mass Mechanical Loads in Electric Drives. In *The fourth IEEE Energy Conversion Congress and Exposition (ECCE)*, 8 p., Raleigh, North Carolina, September 2012.

V Lennart Harnefors, Seppo E. Saarakkala, Marko Hinkkanen. Speed

Control of Electric Drives Using Classical Control Methods. *IEEE Transactions on Industry Applications*, Vol. 49, No. 2, pp. 889–898, March-April 2013.

VI Seppo E. Saarakkala, Marko Hinkkanen. Identification of Two-Mass Mechanical Systems in Closed-Loop Speed Control. In *The 39th Annual Conference of the IEEE Industrial Electronics Society (IECON)*, 6 p., Wien, Austria, November 2013.

VII Seppo E. Saarakkala, Marko Hinkkanen. Identification of Two-Mass Mechanical Systems Using Torque Excitation: Design and Experimental Evaluation. In *2014 International Power Electronics Conference (IPEC)*, 8 p., Hiroshima, Japan, May 2014.

VIII Seppo E. Saarakkala, Marko Hinkkanen. State-Space Speed Control of Two-Mass Mechanical Systems: Analytical Tuning and Experimental Evaluation. *IEEE Transactions on Industry Applications*, Early access, 10 p., September-October 2014.

Author's Contribution

Publication I: "Physical Drawbacks of Linear High Speed Tooth Belt Drives"

In this paper, the frictions and flexibility of a high-speed, tooth-belt linear drive system are analyzed and identified using a test system.

Seppo Saarakkala participated in the writing of the paper under the guidance of Dr. Markku Niemelä, Dr. Riku Pöllänen, and Prof. Juha Pyrhönen. Seppo Saarakkala did the friction modeling and the friction compensation part of the paper and completed the theoretical derivation of the position-dependent resonant frequency of the system.

Publication II: "Dynamic Emulation of Multi-Mass Mechanical Loads in Electric Drives"

This paper presents a straightforward method for dynamic emulation of multi-mass systems. The test bench consisted of a driving motor coupled rigidly to a load servo motor, and the torque reference of the servo motor was controlled based on the dynamic model being emulated.

Seppo Saarakkala defined the research problem and wrote the paper in cooperation with Mr. Antti Alahäivälä under the guidance of Prof. Marko Hinkkanen and Prof. Jorma Luomi. Seppo Saarakkala helped with the experimental tests.

Publication III: "Parameter Estimation of Two-Mass Mechanical Loads in Electric Drives"

This paper presents a method for estimating the parameters of two-mass mechanical loads. A discrete-time polynomial model with an output error (OE) structure was used for the parameter estimation.

Seppo Saarakkala defined the research problem and wrote the paper in cooperation with Mr. Tuomo Leppinen under the guidance of Prof. Marko Hinkkanen and Prof. Jorma Luomi.

Publication IV: "Speed Control of Two-Mass Mechanical Loads in Electric Drives"

This paper deals with model-based, two-degrees-of-freedom (2DOF) speed control of two-mass systems. An analytic gain selection of a proportional-integral (PI) type feedback controller is proposed. The gains are given as functions of system parameters and desired dominant closed-loop poles.

Seppo Saarakkala wrote the paper under the guidance of Prof. Marko Hinkkanen and Dr. Kai Zenger

Publication V: "Speed Control of Electric Drives Using Classical Control Methods"

A classical control approach to the design and analysis of proportional-integral (PI) speed controllers for electrical drives is presented in this paper. A well-performing, two-degrees-of-freedom (2DOF) PI controller is designed using an analytical parameter selection.

Seppo Saarakkala participated in the writing of the paper under the guidance of Prof. Marko Hinkkanen. Seppo Saarakkala contributed by analyzing and writing the 2DOF speed control design and by conducting the experiments.

Publication VI: "Identification of Two-Mass Mechanical Systems in Closed-Loop Speed Control"

This paper presents a method to identify the parameters of the two-mass mechanical system, when the system is operating in closed-loop speed control.

Seppo Saarakkala wrote the paper under the guidance of Prof. Marko Hinkkanen

Publication VII: "Identification of Two-Mass Mechanical Systems Using Torque Excitation: Design and Experimental Evaluation"

This paper deals with methods for parameter estimation of two-mass mechanical systems in electric drives. The mechanical system was excited using a pseudo-random binary signal (PRBS) and the rotor-speed response of the driving motor was measured. An open-loop identification setup and two closed-speed-loop identification setups (direct and indirect) were designed and experimentally compared.

Seppo Saarakkala wrote the paper under the guidance of Prof. Marko Hinkkanen

Publication VIII: "State-Space Speed Control of Two-Mass Mechanical Systems: Analytical Tuning and Experimental Evaluation"

This paper presents a model-based, two-degrees-of-freedom (2DOF), state-space speed control of a two-mass system. Analytical tuning rules for a feedback gain, a state observer, and a prefilter were derived.

Seppo Saarakkala wrote the paper under the guidance of Prof. Marko Hinkkanen

Symbols and Abbreviations

Abbreviations

ARX	Autoregressive with exogenous inputs
ARMAX	Autoregressive moving average with exogenous inputs
ac	Alternative current
DTC	Direct torque control
dc	Direct current
FOC	Field oriented control
OE	Output error
PI	Proportional integral
PID	Proportional integral derivative
PMSM	Permanent-magnet synchronous motor
PRBS	Pseudo-random-binary signal
1DOF	One-degree-of-freedom
2DOF	Two-degrees-of-freedom

Transfer functions

Boldface symbol indicates a multiple-input-multiple-output system

$A_{\mathrm{d}}(z)$, $B_{\mathrm{L,d}}(z)$, $B_{\mathrm{M,d}}(z)$	Discrete-time transfer function polynomials
$A_{\mathrm{f}}(z)$	Discrete-time filtering polynomial
$C(s)$	Feedback controller
$\boldsymbol{F}(s)$	Prefilter
$\boldsymbol{F}_{\mathrm{PI}}(s)$	Prefilter for PI-controlled system
$\boldsymbol{F}_{\mathrm{sfb}}(s)$	Prefilter for state-feedback-controlled system
$\boldsymbol{F}_{\mathrm{f}}(s)$	Feedforward controller

$G(s)$	Open-loop single-mass system
$\boldsymbol{G}_{\mathrm{c}}(s)$	Command-tracking transfer function
$G_{\mathrm{d}}(z)$	Discrete-time open-loop two-mass system
$G_{\mathrm{e}}(s)$	Speed observer
$G_{\mathrm{f}}(s)$	Low-pass filter
$G_{\mathrm{fb}}(s)$	Feedback-loop transfer function
$G_{\mathrm{l}}(s)$	Closed-loop load-disturbance rejection transfer function
$G_{\mathrm{L}}(s)$, $G_{\mathrm{M}}(s)$, $G_{\mathrm{ML}}(s)$	Two-mass system open-loop transfer functions
$G_{\mathrm{t}}(s)$	Closed torque-control loop transfer function
$H(s)$	Loop transfer function
$M(s)$	Measurement transfer function
$N(s)$	Measurement-noise amplification

Symbols

A	Closed-loop coefficient
$\boldsymbol{A}$, $\boldsymbol{B}_{\mathrm{u}}$, $\boldsymbol{B}_{\mathrm{w}}$, $\boldsymbol{C}$	Two-mass system open-loop state matrices
a_{ref}	Acceleration reference
$\boldsymbol{A}_{\mathrm{c}}$, $\boldsymbol{B}_{\mathrm{c}}$, $\boldsymbol{C}_{\mathrm{c}}$, $\boldsymbol{D}_{\mathrm{c}}$	2DOF controller state matrices
$\boldsymbol{A}_{\mathrm{cl}}$, $\boldsymbol{B}_{\mathrm{cl,r}}$, $\boldsymbol{B}_{\mathrm{cl,L}}$, $\boldsymbol{C}_{\mathrm{L}}$	Closed-loop state matrices
$\boldsymbol{A}_{\mathrm{f}}$, $\boldsymbol{B}_{\mathrm{f}}$, $\boldsymbol{C}_{\mathrm{f}}$, $\boldsymbol{D}_{\mathrm{f}}$	Prefilter state matrices
$\boldsymbol{A}_{\mathrm{o}}$	Full-order observer state matrix
$\boldsymbol{A}_{\mathrm{r}}$, $\boldsymbol{B}_{\mathrm{r}}$, $\boldsymbol{B}_{\mathrm{y}}$	Reduced-order observer state matrices
a_1, a_2, a_3, b_1, b_2, b_3	Continuous-time transfer function coefficients
b, b_{L}, b_{M}	Viscous-friction coefficient
c_{S}, c_{S1}, c_{S2}	Torsional damping
d_{i}, d_{o}	Shaft diameter
e	Output noise
F_{i}	Initial-tension force
G	Shear modulus of elasticity
h	Sampling time
$\boldsymbol{I}$	Identity matrix
I_{s}	Torsion modulus
J	Total moment of inertia
J_{L}, J_{L1}, J_{L2}	Load moment of inertia
J_{M}	Motor moment of inertia
j	Imaginary unit

j_{ref}	Jerk reference
k	discrete-time instant
k_{i}	Integral gain
k_{p}	Proportional gain
K_{S}, K_{S1}, K_{S2}	Torsional stiffness
$K_{\mathrm{S,l}}$	Spring constant
k_1, k_2, k_3	State-feedback gains
$\boldsymbol{L}$	Full-order observer gain vector
l_{b}	Distance between belt pulleys
l_{d}	Disturbance-observer gain
l_{e}	Speed-observer gain
l_{f1}, l_{f2}, l_{f3}	Full-order observer gains
$\boldsymbol{L}_{\mathrm{r}}$	Reduced-order observer gain vector
l_{r1}, l_{r2}	Reduced-order observer gains
l_{s}	Shaft length
M_{S}	Sensitivity-function peak
n	Speed-measurement noise
n_{pp}	Speed-measurement noise peak-to-peak amplitude
Q_{k}	Coupling-type dependent damping constant
R	Inertia ratio
R_{ε}	Autocorrelation of residuals
$R_{\varepsilon,u}$	Cross-correlation between input and residuals
r_{p}	Radius of the belt pulley
s	Laplace-domain variable
t	Continuous time
T_{c}	Speed-controller output
$T_{\mathrm{c,sat}}$	Saturated speed-controller output
$T_{\mathrm{c,max}}$	Maximum torque
T_{d}	Torque-control loop delay
T_{ff}	Feedforward torque
T_{g}	Gravitation torque
T_{L}, T_{LM}, T_{L1}, T_{L2}	Loading torque
T_{M}	Motor torque
$T_{\mathrm{M,ref}}$	Motor-torque reference
T_{m}	Speed measurement delay
T_{S}, T_{S1}, T_{S2}	Shaft torsional torque
u	Excitation signal
$\boldsymbol{u}_{\mathrm{c}}$	2DOF controller input vector

$\boldsymbol{x}$	Two-mass system open-loop state vector
$\boldsymbol{x}_\mathrm{c}$	2DOF controller state vector
$\boldsymbol{x}_\mathrm{cl}$	Closed-loop state vector
$\boldsymbol{x}_\mathrm{f}$	Prefilter state vector
x_I	Integral state
$\boldsymbol{x}_\mathrm{r}$, $\boldsymbol{x}_\mathrm{ro}$	Reduced-order observer state vectors
y	Output signal
y_f	Filtered output signal
z	Time-shift operator
α, β, γ	Prefilter coefficients
α_c	Current-control loop bandwidth
α_f	Low-pass filter cut-off frequency
α_s	Speed-control loop bandwidth
α_t	Torque-control loop bandwidth
$\Delta\phi$	Incremental-encoder resolution
ϵ	Tensile strain
ε	Residual
ζ_d, ζ_l, ζ_r	Relative damping
$\boldsymbol{\theta}$	Parameter vector
θ_L, θ_1, θ_2	Load angular position
θ_M	Motor angular position
$\boldsymbol{\phi}$	Predictor vector
$\boldsymbol{\Phi}_\mathrm{c}$, $\boldsymbol{\Gamma}_\mathrm{c}$, $\boldsymbol{H}_\mathrm{c}$, $\boldsymbol{J}_\mathrm{c}$	Discrete-time 2DOF controller state matrices
$\boldsymbol{\phi}_\mathrm{f}$	Filtered predictor vector
ω	Angular frequency
ω_ares	Antiresonance frequency
ω_d, ω_l, ω_r	Undamped natural frequency
ω_L, ω_1, ω_2	Load angular speed
ω_M	Measured motor angular speed
ω'_M	Motor angular speed
$\omega_\mathrm{M,f}$	Filtered motor angular speed
ω_ref, $\omega_\mathrm{ref,filt}$	Speed reference
ω_res	Resonance frequency

1. Introduction

1.1 Background

Electrical machines have been increasingly applied to generate mechanical motion since the beginning of the 1970s, due to the rapid development of power-electronic devices. The term "mechatronics" has been a registered trademark of the Yaskawa Electric Corporation since 1971 [1]. This trademark clearly already indicated at the time that many more electrical devices would be developed in the future in the mechanical engineering field. The power-electronic devices were applied together with direct-current (dc) machines in the form of dc/dc converters. For dc machines, a very quick and accurate torque response can be accomplished by maintaining a constant flux and varying the armature current via closed-loop control. However, it was the development of vector-control methods for alternative-current (ac) machines that triggered a sustained increase in the number of emerging applications for electrical machines in the mechatronic field. These vector-control methods include field-oriented control (FOC) [2] and direct torque control (DTC) [3, 4]. Nowadays, high-performance ac electric drives are replacing pneumatic and hydraulic actuators or dc motor drives in modern machineries—such as injection molding machines [5], machine tools [6, 7], and industrial robots [8, 9]—due to their energy efficiency, compact size, and flexible control algorithms. These machineries often consist of several moving or rotating masses, which are coupled together with flexible mechanical transmissions (e.g., belts, gearboxes, long shafts), leading to mechanical resonances [1]. To achieve high dynamic performance, the motion control of the drive systems with resonant mechanical loads should be based on higher-order system models.

The most simple simple way of controlling the rotational speed of an ac electrical-motor-driven system is through controlling the stator voltage in proportion to the supply frequency. This very simple open-loop control method, also known as constant voltage-per-hertz (u/f) control, was used especially during the 1980s. However, the dynamics of the speed control are not satisfactory for motion control purposes when applying the u/f control. The development of vector-control methods made it possible to clearly separate the faster electrical phenomena (i.e., flux and torque dynamics) from the slower mechanical phenomena.

Due to improved motor control and increased computational power, more effort was directed towards motion control development [1]. The proportional-integral (PI) type controller is the most widely used speed-feedback controller. During the 1980s, the PI speed control was proposed for dc machines [10] and also for ac machines together with FOC [11] and DTC [12]. Two-degrees-of-freedom (2DOF) motion control methods, where regulation and command tracking properties are designed separately, have been proposed in several studies [13, 14]. During the late 1980s and early 1990s, the control of resonant mechanical systems was introduced. The first reported methods included the use of additional feedback [15], load-torque estimation [16], and state-space control [17–19]. Later on, the proposed methods also included the use of nonlinear and adaptive controllers [20]. However, as stated in [21], a properly tuned classical PI or PI derivative (PID) controller is still an appropriate selection even today. Nowadays, the resonant mechanical systems are commonly controlled by means of a model-based, two-degrees-of-freedom control, where regulation and command tracking properties are separately designed [22]. However, tuning these controllers is not always straightforward, and if the speed-feedback loop is delayed and noisy, even the stability may be lost if the feedback controller is not properly tuned. Thus, a demand for further developing automatically-tuned, robust, model-based motion controllers still exists.

Model-based automatic controller tuning typically relies on having knowledge of the mechanical parameters and some performance specifications (e.g., closed-loop bandwidth) [23, 24]. However, datasheets on the mechanical components are not often available or else calculating the mechanical parameters can be a highly complex task. Hence, to enable model-based automatic tuning of the motion controllers, the mechanical parameters should be identified during the start-up of a drive or during

the drive operation. Moreover, the process of identifying the mechanical system may offer a possibility to diagnose mechanical faults. As an example, a method to detect a rolling bearing damage has been proposed in [25].

Because of increasing interest in model-based, self-tuning control structures, the identification of mechanical systems in electrical drives became a popular topic in the late 1990s. In general, the mechanical system can be identified using either frequency-domain or time-domain observations [26]. It is evident that if frequency-domain methods are applied, the measured data must be available in the frequency domain. However, the measured signals are usually collected as a time series, meaning that the time-domain data must be converted into the frequency domain using some specified algorithm. This conversion process always leads to an extra calculation step and the accuracy depends on the conversion method [27]. Moreover, if the physical parameters of the system are of interest, an additional parameter-fitting algorithm is needed. Despite these drawbacks, the frequency-domain estimation methods are also widely applied [28,29]. On the other hand, when applying discrete-time polynomial-based identification methods, the polynomial coefficients can be directly estimated based on the collected data set [30, 31]. However, the polynomial-model structure and the model degree need to be decided before the identification process. Furthermore, if the physical parameters are of interest, the discrete-time polynomial coefficients need to be converted into the continuous-time domain. Completing the conversion numerically is a straightforward task, but finding analytical relations can be tricky.

1.2 Objective and Outline of the Dissertation

The aim of this dissertation is to develop robust analytical tuning rules for the motion-controller gains in electrical drives. For the sake of applicability, these tuning rules have been developed for classical controllers, such as PI control and observer-based, state-space control. Because the controller gains are analytically parametrized in the mechanical parameters of the controlled load, the tuning rules can be applied for a gain-scheduled controller without difficulties.

Because the mechanical parameters are not always available or may be difficult to calculate, this dissertation provides a method to identify the controlled mechanical load. As an output of the identification method,

the mechanical parameters of the controlled load are obtained as analytical relations. A straightforward automatic tuning of the motion controller can be obtained when the parameter-identification method and the model-based controller are applied together.

Section 2 introduces the most common mathematical models related to the speed control of electric drives, while Section 3 describes the control methods that utilize these models. Section 4 introduces methods to identify the parameters of the mathematical models and Section 5 describes the experimental setups applied for testing. A summary and abstracts of the publications are provided in Section 6, followed by concluding remarks in Section 7.

2. System Modeling

The mechanical dynamics of a rotating electrical-drive system can be derived from Newton's law of rotating bodies. Publication I deals with the modeling issues and difficulties related to multi-mass mechanical loads in electric drives. This chapter introduces the most important mathematical models. The mechanical dynamics can be modeled using the motor inertia J_{M} and distributed load inertias $\{J_{\mathrm{L}},\, J_{\mathrm{L1}},\, J_{\mathrm{L2}}\}$. The motor and load inertias are connected using springs $\{K_{\mathrm{S}},\, K_{\mathrm{S1}},\, K_{\mathrm{S2}}\}$ and dampers $\{c_{\mathrm{S}},\, c_{\mathrm{S1}},\, c_{\mathrm{S2}}\}$. The more load inertias are modeled, the more accurate the system model, but the trade-off is that at the same time the complexity and degree of the model increase. Fig. 2.1 depicts the three mechanical models considered in this study.

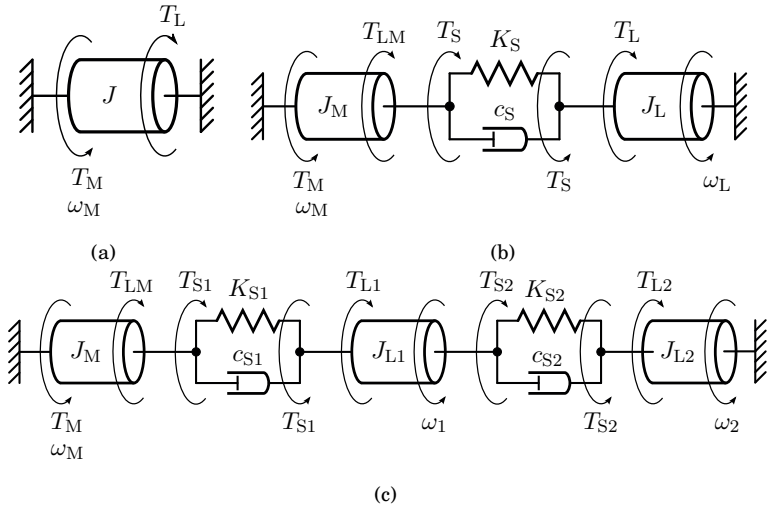

Figure 2.1. System models: (a) Single-mass system; (b) two-mass system; and (c) three-mass system.

2.1 Single-Mass Model

The model of a single-mass mechanical system, shown in Fig. 2.1(a), is given as follows:

$$J\frac{d\omega_{\mathrm{M}}}{dt} = T_{\mathrm{M}} - T_{\mathrm{L}} \tag{2.1}$$

where J is the total moment of inertia of the system. The torque and the angular speed of the motor are T_{M} and ω_{M}, respectively. The net-loading torque is denoted as T_{L}. If $T_{\mathrm{L}} = b\omega_{\mathrm{M}}$ is assumed, then the single-mass system (2.1) can be presented in the Laplace domain as a first-order transfer function from T_{M} to ω_{M}:

$$G(s) = \frac{1}{Js + b} \tag{2.2}$$

where b is the coefficient of the viscous friction acting on the system.

2.2 Two-Mass Model

The model of a two-mass mechanical system, shown in Fig. 2.1(b), is given as follows:

$$J_{\mathrm{M}}\frac{d\omega_{\mathrm{M}}}{dt} = T_{\mathrm{M}} - T_{\mathrm{LM}} - T_{\mathrm{S}} \tag{2.3a}$$

$$J_{\mathrm{L}}\frac{d\omega_{\mathrm{L}}}{dt} = T_{\mathrm{S}} - T_{\mathrm{L}} \tag{2.3b}$$

$$T_{\mathrm{S}} = K_{\mathrm{S}}(\theta_{\mathrm{M}} - \theta_{\mathrm{L}}) + c_{\mathrm{S}}(\omega_{\mathrm{M}} - \omega_{\mathrm{L}}) \tag{2.3c}$$

where J_{L} is the inertia on the load. The angular speeds of the motor and the load are ω_{M} and ω_{L}, respectively. The angular positions of the motor and load are θ_{M} and θ_{L}, respectively. The angular speeds are the first time derivatives of the angular positions: $\omega_{\mathrm{M}} = d\theta_{\mathrm{M}}/dt$ and $\omega_{\mathrm{L}} = d\theta_{\mathrm{L}}/dt$. The loading torques acting on the motor and on the load are denoted as T_{LM} and T_{L}, respectively.

If $T_{\mathrm{LM}} = 0$ is assumed, then the mechanical dynamics of the resonating two-mass system (2.3) can be given as a state-space representation:

$$\dot{\boldsymbol{x}} = \underbrace{\begin{bmatrix} -\frac{c_{\mathrm{S}}}{J_{\mathrm{M}}} & -\frac{K_{\mathrm{S}}}{J_{\mathrm{M}}} & \frac{c_{\mathrm{S}}}{J_{\mathrm{M}}} \\ 1 & 0 & -1 \\ \frac{c_{\mathrm{S}}}{J_{\mathrm{L}}} & \frac{K_{\mathrm{S}}}{J_{\mathrm{L}}} & -\frac{c_{\mathrm{S}}}{J_{\mathrm{L}}} \end{bmatrix}}_{\boldsymbol{A}} \boldsymbol{x} + \underbrace{\begin{bmatrix} \frac{1}{J_{\mathrm{M}}} \\ 0 \\ 0 \end{bmatrix}}_{\boldsymbol{B}_{\mathrm{u}}} T_{\mathrm{M}} + \underbrace{\begin{bmatrix} 0 \\ 0 \\ -\frac{1}{J_{\mathrm{L}}} \end{bmatrix}}_{\boldsymbol{B}_{\mathrm{w}}} T_{\mathrm{L}} \tag{2.4}$$

where $\boldsymbol{x} = \begin{bmatrix} \omega_{\mathrm{M}} & \theta_{\mathrm{M}} - \theta_{\mathrm{L}} & \omega_{\mathrm{L}} \end{bmatrix}^{\mathrm{T}}$. The transfer function from T_{M} to ω_{M} is

$$G_{\mathrm{M}}(s) = \begin{bmatrix} 1 & 0 & 0 \end{bmatrix} (s\boldsymbol{I} - \boldsymbol{A})^{-1} \boldsymbol{B}_{\mathrm{u}} \tag{2.5}$$

The transfer function from T_L to ω_M is

$$G_\mathrm{L}(s) = \begin{bmatrix} 1 & 0 & 0 \end{bmatrix} (s\boldsymbol{I} - \boldsymbol{A})^{-1} \boldsymbol{B}_\mathrm{w} \tag{2.6}$$

and the transfer function from T_M to ω_L is

$$G_\mathrm{ML}(s) = \begin{bmatrix} 0 & 0 & 1 \end{bmatrix} (s\boldsymbol{I} - \boldsymbol{A})^{-1} \boldsymbol{B}_\mathrm{u} \tag{2.7}$$

If torsional damping $c_\mathrm{S} = 0$ is assumed, then the antiresonance and resonance frequencies are

$$\omega_\mathrm{ares} = \sqrt{\frac{K_\mathrm{S}}{J_\mathrm{L}}} \tag{2.8a}$$

$$\omega_\mathrm{res} = \sqrt{K_\mathrm{S} \frac{J_\mathrm{M} + J_\mathrm{L}}{J_\mathrm{M} J_\mathrm{L}}} \tag{2.8b}$$

respectively.

2.3 Three-Mass Model

The model of a three-mass mechanical system, shown in Fig. 2.1(c), is given as follows:

$$J_\mathrm{M} \frac{d\omega_\mathrm{M}}{dt} = T_\mathrm{M} - T_\mathrm{LM} - T_\mathrm{S1} \tag{2.9a}$$

$$J_\mathrm{L1} \frac{d\omega_1}{dt} = T_\mathrm{S1} - T_\mathrm{L1} - T_\mathrm{S2} \tag{2.9b}$$

$$J_\mathrm{L2} \frac{d\omega_2}{dt} = T_\mathrm{S2} - T_\mathrm{L2} \tag{2.9c}$$

$$T_\mathrm{S1} = K_\mathrm{S1}(\theta_\mathrm{M} - \theta_1) + c_\mathrm{S1}(\omega_\mathrm{M} - \omega_1) \tag{2.9d}$$

$$T_\mathrm{S2} = K_\mathrm{S2}(\theta_1 - \theta_2) + c_\mathrm{S2}(\omega_1 - \omega_2) \tag{2.9e}$$

where J_L1 is the first-load inertia and J_L2 is the second-load inertia. The angular speeds of the motor and the loads are ω_M, ω_1, and ω_2, respectively. The angular positions of the motor and loads are θ_M, θ_1, and θ_2, respectively. The loading torques acting on the motor and on the loads are denoted as T_LM, T_L1, and T_L2, respectively.

As an example, an elevator may be modeled as a three-mass system, as shown in Publication II and in [32]. The system model consists of the masses of the cage and the counterweight as well as the inertia of the sheave. A three-mass system model of a linear tooth-belt drive is introduced in Publication I. Publication I likewise demonstrated how to reduce the three-mass system model to the two-mass model. A three-mass system model of a linear lead-screw drive can be found in [33].

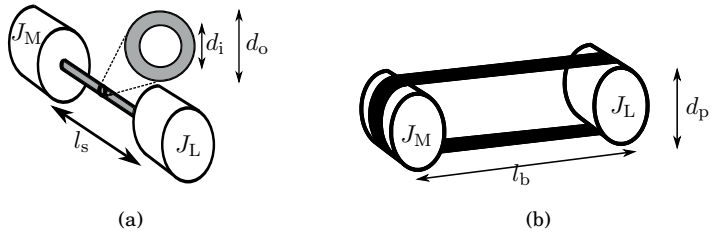

Figure 2.2. Two-inertia system configurations: (a) Inertias are coupled with a long shaft; (b) inertias are coupled with a belt.

2.4 Spring Constants

The spring constants of the two- or multi-mass systems may be estimated using the manufacturer's datasheets. Fig 2.2 shows two different two-inertia system configurations. In Fig. 2.2(a), a long shaft is used to couple the inertias, whereas in Fig. 2.2(b), a belt is used to couple the inertias. The analytical calculation of the spring constants depends on the coupling type and the material used for the coupling.

The spring constant of a shaft-coupled two-inertia system [shown in Fig. 2.2(a)] can be calculated as follows [34]:

$$K_{\mathrm{S}} = \frac{GI_{\mathrm{s}}}{l_{\mathrm{s}}} \tag{2.10}$$

where G is the shear modulus of elasticity of the shaft material, I_{s} is the torsion modulus, and l_{s} is the length of the shaft. The torsion modulus of a hollow shaft can be calculated as follows [34]:

$$I_{\mathrm{s}} = \frac{\pi \left(d_{\mathrm{o}}^4 - d_{\mathrm{i}}^4\right)}{32} \tag{2.11}$$

where d_{o} and d_{i} are the outer and inner diameters of the shaft, respectively. It is worth noticing that the torsion modulus of a solid shaft may be calculated by substituting $d_{\mathrm{i}} = 0$ into (2.11).

Publication I showed that the spring constants of a tooth-belt-driven system [shown in Fig. 2.2(b)] can be derived from Hooke's law as

$$K_{\mathrm{S,l}} = \frac{2F_{\mathrm{i}}}{\epsilon l_{\mathrm{b}}} \tag{2.12}$$

where F_{i} is the initial-tension force of the belt, ϵ is the tensile strain of the belt at the initial force, and l_{b} is the length between the belt pulleys [see Fig. 2.2(b)]. It should be noted that (2.12) gives the spring constant for linear motion. If this spring constant is to be used in rotational-system equations [(2.3c), (2.9d), or (2.9e)], it should be scaled with the radius of the belt pulley r_{p} as $K_{\mathrm{S}} = r_{\mathrm{p}}^2 K_{\mathrm{S,l}}$.

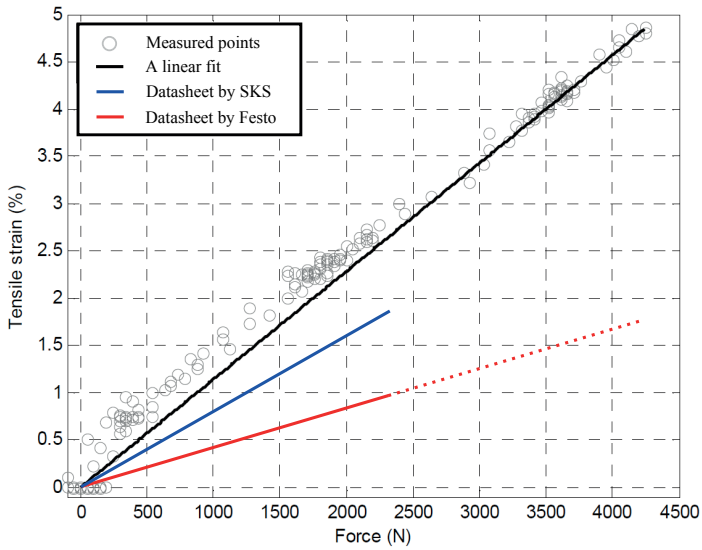

Figure 2.3. Stretching characteristics of the belt from the experimental setup used in Publication I and in [35, 36].

Equations (2.10) and (2.12) demonstrate that the spring constants depend on the material properties and on the length of the coupling. Typically, if shaft coupling is applied, then the material of the shaft is known and calculating the spring constant is a relatively straightforward process. On the other hand, for the tooth-belt connected inertias, Publication I demonstrated that it may be difficult to find values for the belt characteristics F_{i} and ε.

Fig. 2.3 shows two datasheet-based characteristics of as well as experimental-based stretching characteristics of a tooth belt. The datasheet values were provided by Festo Oy and SKS Group Oy. Figure shows that three different tensile-strain values can be obtained for the same stretching force. This indicates that it may sometimes be problematic to find accurate values for the mechanical parameters if relying solely on the manufacturer's datasheets. Furhermore, Fig. 2.4 shows the stretching characteristics (provided by SKS Group Oy) of the belts from the experimental setup described in Section 5.1.

Both Publication I and [36] showed that if a linearly-moving mass is attached between the rotational masses of the tooth-belt driven system, depicted in Fig. 2.2(b), then the spring constants of the system will become nonlinearly dependent on the position of that mass. The same kind of position-dependent spring constants can be found in elevators [32] or in lead-screw drives [33].

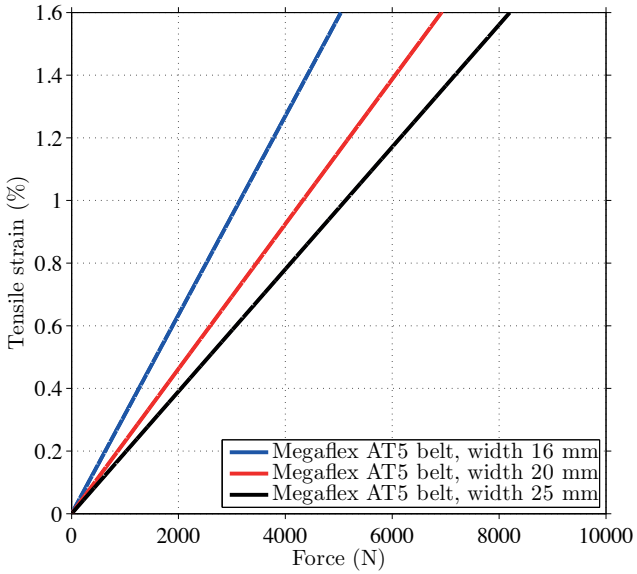

Figure 2.4. Datasheet-based stretching characteristics of the belt from the experimental setup used in Publication IV, Publication VII, and Publication VIII.

According to [37], the torsional damping c_{S} can be approximated as

$$c_{\mathrm{S}} = \frac{K_{\mathrm{S}}}{\omega_{\mathrm{res}} Q_{\mathrm{k}}} \tag{2.13}$$

where ω_{res} is the resonance frequency of the system [see (2.8)]. The coefficient Q_{k} depends on the coupling type. As an example, the reference [37] advises selecting $Q_{\mathrm{k}} = 10$ for flexible couplings.

2.5 Torque Production of an Electrical Motor

When the torque control of the ac motor is realized using the vector-control methods or when the dc motor is applied, and the system is operating in the linear region, then the closed torque-control loop can be modeled as a transfer function from the torque reference $T_{\mathrm{M,ref}}$ to the actual motor torque T_{M} [38]:

$$G_{\mathrm{t}}(s) = e^{-sT_{\mathrm{d}}} \frac{\alpha_{\mathrm{t}}}{s + \alpha_{\mathrm{t}}} \tag{2.14}$$

where α_{t} is the bandwidth and T_{d} is the time delay of the torque-control loop.

Publication V analytically demonstrated that the performance of the speed-control loop does not deteriorate significantly, if $T_{\mathrm{d}} = 0$ is assumed and if the bandwidth α_{t} of the torque-control loop is approximately four

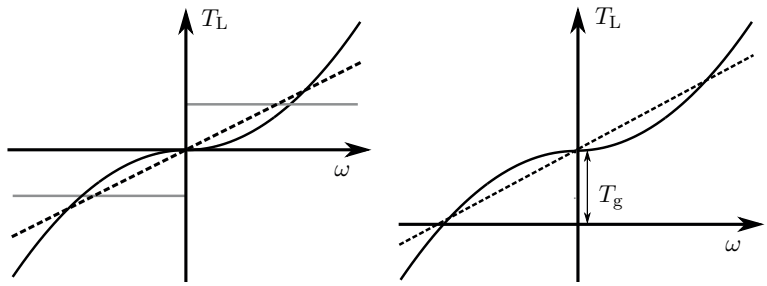

Figure 2.5. Typical load-torque profiles: (a) Coulomb friction (grey), viscous friction (dashed black), and quadratic-load torque (solid black); (b) gravitation torque T_g included.

times greater than the required bandwidth α_s of the speed-control loop. A torque response in the ms range can easily be achieved for a modern electric drive, which is generally several orders of magnitude faster than the closed-loop mechanical dynamics.

2.6 Loading Torque

Many handbooks dealing with electrical drives introduce typical loading-torque profiles. As an example, a work by Leonhard [39] provides a nice overview of loading torque and is referred to in this section, but others can be found as well. Loading torques, acting on different parts of the drive system, may be categorized into two groups: speed-dependent and speed-independent loading torques.

Always, when the mechanical motion (linear or rotational) is generated, a frictional force appears between the surfaces. Frictions can be divided into three different components: Coulomb friction, stiction, and viscous damping. Fig. 2.5 shows the characteristics of different frictions. Fig. 2.5(a) shows that Coulomb (sliding) friction belongs to the speed-independent category because it has a constant value, which changes only when the direction of the motion is changed. Stiction, also known as break-away friction, has a nonzero value only when the motor speed is zero; otherwise, the value of the stiction is zero. Viscous damping (friction) is linearly or quadratically proportional to the velocity. Quadratic-friction torque may appear, for example, in fan applications. If the electrical drive is used in a hoisting application, such as in elevators [32], cranes [40], or vehicles [41], a constant speed-independent gravitational torque appears.

The gravitational torque is depicted in Fig. 2.5(b) and indicated as T_{g}.

In addition to the simple profiles, shown in Fig. 2.5, more advanced load-torque models can be found in the literature. As an example, the frictional torques of a road vehicle are introduced in [41]. The speed-dependent friction torque of a linear tooth-belt drive is shown in [35] and the position dependency of the friction torque for the same device can be found in [36]. An extensive survey of friction modeling, analysis, and compensation methods can be found, for example, in [42].

Moreover, backlash is a quite common nonlinearity that occurs in mechanical systems, especially when a gearbox is used. Backlash means that there is a small movement in the motor until the load moves. A good survey paper about the modeling and control of mechanical systems with backlash has been provided in [43].

Together, these phenomena make the system nonlinear. The identification and control of these nonlinearities are, however, not addressed in this work.

2.7 Speed Measurement

A simple way to measure motor speed is to apply, for example, an incremental encoder. The angular speed is calculated based on the difference in the measured angular position within the fixed sampling interval h. This sampling scheme leads to a significant quantization noise and a measurement delay length of the sampling interval [44]. Thus, the speed measurement may be modeled in the manner depicted in Fig. 2.6. The actual motor speed is denoted as ω'_{M} and the measured speed as ω_{M}. The transfer function $M(s)$ models the known time delay T_{m} as

$$M(s) = e^{-sT_{\mathrm{m}}} \tag{2.15}$$

On the other hand, the quantification noise is modeled as a zero-mean white noise n [see Fig. 2.6]. The peak-to-peak amplitude of the speed-measurement noise may be approximated as $n_{\mathrm{pp}} = \Delta\phi/h$, where $\Delta\phi$ is the resolution of the incremental encoder [45]. It is worth noting that if a more elaborate speed-calculation scheme would be applied, the speed-measurement delay could be reduced to half the sampling period. Furthermore, the measurement-noise amplitude could be significantly reduced [45].

Other speed-measurement devices include, for example, absolute en-

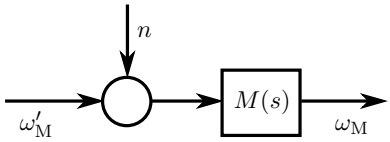

Figure 2.6. Speed-measurement model for an incremental encoder.

coders (both single-turn and multi-turn encoders), sinusoidal encoders, and resolvers.

2.8 Delay and Noise in the Control System

There are several sources for noises and delays in electrical-drive control systems. The delays can be roughly grouped into torque-control loop delays T_d (see Section 2.5), and speed-measurement delays T_m (see Section 2.7). Publication VIII determined that the total feedback-loop delay $T_\mathrm{d} + T_\mathrm{m}$ is the most important parameter when it comes to closed-speed control loop stability. This agrees with the observations made in [36].

If the position/speed control is run in the same device as the torque control (decentralized motion control), the effect of the feedback-loop time delay can be neglected or considered minimal. On the other hand, if the position/speed control is accomplished in a separate micro-processor (centralized motion control) and the torque command $T_\mathrm{M,ref}$ is sent to the torque controller, for example, using a field bus, then the time delay will increase and should be taken into account. The delay of an asychronous Profibus network has been measured in [35]. The delays of a Sercos network have been described in [36]. Furthermore, a significant speed-measurement delay can be present, if the motor-supply cable is used also as a feedback channel [46]. Some examples of the delay sources and the delay lengths have been gathered together in Tables 2.1 and 2.2. More information about the field bus technology used in motion control devices can be found, for example, in [47].

Table 2.1. Current-control loop time delay

Delay source	Delay T_{d} [ms]
FOC [39]	0.2
DTC [39]	0.2
Sercos (0.25 ms cycle time) [36]	0.1
Sercos (0.5 ms cycle time) [36]	0.4
Sercos (1 ms cycle time) [36]	0.9
Profibus [35]	2-4

Table 2.2. Feedback time delay when the sampling time T_{s} is 0.5 ms

Delay source	Delay T_{m} [ms]
Speed measurement 1 [44]	0.25
Speed measurement 2 [45]	0.5
Sercos (0.25 ms cycle time) [36]	0.11
Sercos (0.5 ms cycle time) [36]	0.11
Sercos (1 ms cycle time) [36]	0.11
Profibus [35]	2-4
Supply cable [46]	4-10

3. Model-Based Control

This chapter reviews the most common methods proposed in the literature for speed control of electric drives. To provide some background to control algorithm development, the speed control of a simple single-mass system is first described in Section 3.1. The most attention, however, is paid to the development of control-design methods for two- or multi-mass systems, which are presented at the end of this chapter. All the control methods discussed in this chapter make use of knowledge about the mechanical parameters of the controlled system. These parameters may be obtained from manufacturer's datasheets, or more preferably, from a parameter-estimation routine, as will be described in Chapter 4.

Several publications focus on a particular motor type: a dc motor [48,49], an induction motor [50–61], a permanent-magnet synchronous motor [62–69], or a switched reluctance motor [70, 71]. This is quite surprising because, as was discussed in Section 2.5, the electrical dynamics are transparent when seen from the mechanical side. Further details may be found in Publication V.

The speed control of electrical drives is usually established by means of

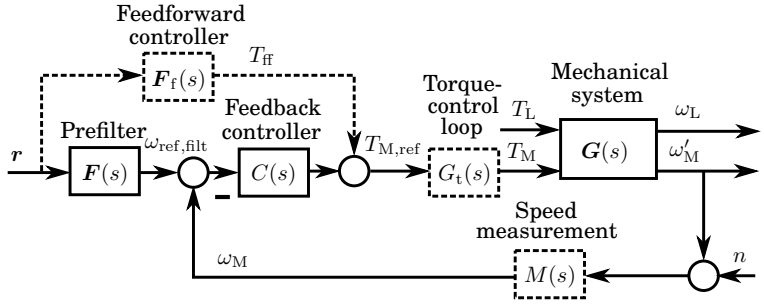

Figure 3.1. 2DOF control structure consisting of the controlled mechanical system $\boldsymbol{G}(s)$, the measurement-transfer function $M(s)$, the closed torque-control loop transfer function $G_{\mathrm{t}}(s)$, the feedback controller $C(s)$, and the prefilter $\boldsymbol{F}(s)$ or feedforward controller $\boldsymbol{F}_{\mathrm{f}}(s)$.

2DOF control (see Fig. 3.1) consisting of a feedback controller $C(s)$, the controlled mechanical system $G(s)$ [(2.2) or (2.5)], and a prefilter $\boldsymbol{F}(s)$ or feedforward controller $\boldsymbol{F}_{\mathrm{f}}(s)$. When the 2DOF controller is applied, the regulation and command tracking can be treated separately [72]. The feedback controller $C(s)$ is used to stabilize the feedback loop and to reject the loading torque (such as friction) acting on the system. If the feedback controller is also designed for command tracking, the feedback gain will increase and stability may be lost. Instead, a prefilter $\boldsymbol{F}(s)$ (or a feedforward controller) inserted into the command path can be used to improve the command-tracking capability. In this study, the prefilter has been designed assuming that a reference vector $\boldsymbol{r} = \begin{bmatrix} j_{\mathrm{ref}} & a_{\mathrm{ref}} & \omega_{\mathrm{ref}} \end{bmatrix}^{\mathrm{T}}$ is available. The speed reference ω_{ref} and its first and second time derivatives a_{ref} and j_{ref}, respectively, can be generated applying input-command shaping techniques (see Section 3.5).

Furthermore, it is beneficial to analyze the effects of the torque-control loop $G_{\mathrm{t}}(s)$ and the speed measurement $M(s)$ (see Sections 2.5, 2.7, and 2.8 for further details). This is especially important if the torque-control loop is slow or if there is a time delay between the torque reference $T_{\mathrm{M,ref}}$ and the actual motor torque T_{M} or if the speed measurement is delayed and noisy.

The speed control has been designed in the following sections by assuming that the load speed ω_{L} should track the reference as accurately as possible. However, the speed control design has been carried out by assuming that only the motor speed ω_{M} is available as the feedback signal. The most important transfer functions regarding the speed control design are as follows:

- The command-tracking transfer function from the reference vector $\boldsymbol{r}$ to the load speed ω_{L}, denoted as $\boldsymbol{G}_{\mathrm{c}}(s)$. This has been designed in the following sections by assuming an ideal torque-control loop and an ideal speed measurement dynamics, that is to say $G_{\mathrm{t}}(s) = M(s) = 1$.

- The closed-loop, load-disturbance rejection transfer function from the loading torque T_{L} to the load speed ω_{L}, denoted as $G_{\mathrm{l}}(s)$. This has been designed in the following sections by assuming that $G_{\mathrm{t}}(s) = M(s) = 1$.

- The loop transfer function $H(s) = G(s)M(s)C(s)G_{\mathrm{t}}(s)$.

- The noise transfer function $N(s)$ from the measurement noise n to the motor torque T_{M}, which is defined as $N(s) = -M(s)C(s)G_{\mathrm{t}}(s)$.

The stability of the different systems will be analyzed in the following sections by means of Nyquist diagrams of the loop transfer functions. The Nyquist diagrams are depicted between the frequencies $\omega = 0$ and $\omega = \pi/h$, where h is the sampling interval of the discrete-time equivalent controller. The Nyquist diagram indicates a stable system if the loop gain does not encircle the critical point $(-1+\mathrm{j}0)$ [73]. A longer distance between the loop transfer function curve and the critical point indicates a more robust feedback loop. Furthermore, the measurement-noise amplification of the different systems are analyzed using the noise transfer functions. A lower measurement-noise amplification indicates a better feedback-loop operation.

3.1 Single-Mass Systems

As mentioned previously, a 2DOF control structure is a popular and effective solution for the speed/position control of electric drives and it is widely applied for single-mass systems using both continuous-time domain and discrete-time domain design techniques [13,48,50–52,62,70,74].

Alternative methods include the usage of a phase-locked loop [53], auto-disturbance rejection [54], load-torque estimation and feedforward [63], and adaptive techniques [64, 66]. Various nonlinear methods, including fuzzy logic [55, 56, 65–67, 75], neural networks [57, 58, 68], and sliding mode (variable structure) control [49, 59–61, 69, 71, 76], have also been proposed. Reference [77] has provided a comparison of PI and fuzzy speed controllers.

3.1.1 Feedback Controller Design

This section presents methods for tuning a model-based, PI speed-feedback controller for a single-mass mechanical system [see (2.2)] When using the PI feedback controller,

$$C(s) = k_{\mathrm{p}} + \frac{k_{\mathrm{i}}}{s} \tag{3.1}$$

where k_{p} is the proportional gain and k_{i} is the integral gain, while the closed feedback-loop transfer function from the loading torque T_{L} to the

motor speed ω_M is

$$G_\mathrm{l}(s) = -\frac{s}{Js^2 + (b + k_\mathrm{p})s + k_\mathrm{i}} \tag{3.2}$$

and from the speed reference $\omega_\mathrm{ref,filt}$ to the motor speed ω_M is

$$G_\mathrm{fb}(s) = \frac{k_\mathrm{p}s + k_\mathrm{i}}{Js^2 + (b + k_\mathrm{p})s + k_\mathrm{i}} \tag{3.3}$$

Equations (3.2) and (3.3) show that the closed-loop system has two poles, and because the controller have two adjustable gains, the locations of these poles can be arbitrarily selected. If $b = 0$ is assumed and the gains are selected as

$$k_\mathrm{p} = 2\zeta_\mathrm{d}\omega_\mathrm{d}J \tag{3.4}$$

$$k_\mathrm{i} = \omega_\mathrm{d}^2 J \tag{3.5}$$

then the denominators of the closed-loop transfer function will be equal to the denominators in a standard second-order transfer function:

$$G_\mathrm{l}(s) = -\frac{s}{J(s^2 + 2\zeta_\mathrm{d}\omega_\mathrm{d}s + \omega_\mathrm{d}^2)} \tag{3.6}$$

$$G_\mathrm{fb}(s) = \frac{2\zeta_\mathrm{d}\omega_\mathrm{d}s + \omega_\mathrm{d}^2}{s^2 + 2\zeta_\mathrm{d}\omega_\mathrm{d}s + \omega_\mathrm{d}^2} \tag{3.7}$$

where ω_d is the undamped natural frequency and ζ_d is the relative damping. Complex-conjugated poles with a negative real part are obtained for $0 < \zeta_\mathrm{d} < 1$. Letting $\zeta_\mathrm{d} = 1$ yields a so-called critically damped system with a double pole at $s = -\omega_\mathrm{d}$. Letting $\zeta_\mathrm{d} > 1$ gives an overdamped system with one “fast" and one “slow" pole (both real), but it is not recommended.[1]

3.1.2 Prefilter or Feedforward Design

The command-tracking dynamics of the system can be designed by first selecting the closed-loop transfer function $\boldsymbol{G}_\mathrm{c}(s)$ from the reference vector $\boldsymbol{r}$ to the load speed ω_L. A first-order, command-tracking transfer function was proposed in Publication V:

$$\boldsymbol{G}_\mathrm{c}(s) = \begin{bmatrix} 0 & 1 & \omega_\mathrm{l} \end{bmatrix} \frac{1}{s + \omega_\mathrm{l}} \tag{3.8}$$

where ω_l is the natural frequency of the first-order pole. This pole can be used to freely select the command-tracking dynamics of the system.[2] More

[1] The relationship between the standard second-order transfer function and the pole selection proposed in Publication V can be given as $\alpha_\mathrm{s} = 2\zeta_\mathrm{d}\omega_\mathrm{d}$.

[2] The relationship between the command-tracking pole selection given here and the pole selection proposed in Publication V can be given as $\omega_\mathrm{l} = n\alpha_\mathrm{s}$.

information about the speed-reference generation can be found in Section 3.5.

The prefilter $\boldsymbol{F}(s)$ or transfer function $\boldsymbol{F}_{\mathrm{f}}(s)$ of the feedforward controller can be then solved by making (3.8) and the following two equations equal to one another:

$$\boldsymbol{G}_{\mathrm{c}}(s) = \frac{\boldsymbol{F}_{\mathrm{f}}(s)G(s) + \begin{bmatrix} 0 & 0 & 1 \end{bmatrix} C(s)G(s)}{1 + C(s)G(s)} \tag{3.9}$$

$$\boldsymbol{G}_{\mathrm{c}}(s) = \boldsymbol{F}(s)G_{\mathrm{fb}}(s) \tag{3.10}$$

When the feedback-controller is of the PI type, the zero and the poles of (3.7) are cancelled out, and the prefilter transfer function from $\boldsymbol{r}$ to $\omega_{\mathrm{ref,filt}}$ becomes

$$\boldsymbol{F}(s) = \begin{bmatrix} 0 & 1 & \omega_{\mathrm{l}} \end{bmatrix} \frac{s^2 + 2\zeta_{\mathrm{d}}\omega_{\mathrm{d}}s + \omega_{\mathrm{d}}^2}{(2\zeta_{\mathrm{d}}\omega_{\mathrm{d}}s + \omega_{\mathrm{d}}^2)(s + \omega_{\mathrm{l}})} \tag{3.11}$$

It is worth noting that equivalent dynamic-reference tracking can be obtained for a single-mass system if an acceleration-feedforward structure is applied. In the acceleration feedforward, a feedforward torque

$$T_{\mathrm{ff}} = Ja_{\mathrm{ref}} = \begin{bmatrix} 0 & J & 0 \end{bmatrix} \boldsymbol{r} \tag{3.12}$$

is added to the output of the feedback controller $C(s)$ [see Fig. 3.1]. The total inertia of the system is denoted as J. This is a well-known method in industrial applications [78]. However, unlike the prefilter (3.11), the acceleration feedforward does not improve step-reference tracking.

3.1.3 Robustness and Measurement-Noise Amplification

Equation (3.1) demonstrates that at higher frequencies (i.e., when $s = j\omega$ increases), the P part of the controller becomes dominant. Usually measurement noise appears in the high-frequency region, meaning that k_{p} mainly defines the measurement-noise amplification of the controller. If the amplitude of the measurement noise is high, it means that in order not to exceed a certain level of noise in the torque reference, the control designer has to reduce either the natural frequency or the damping of the closed-loop poles [see (3.4)]. Another possibility is to reduce the noise before feeding the measured speed back to the controller. Typically, this is done by filtering the measured signal, for instance by applying a first- or second-order low-pass filter. However, filtering the signal may cause problems, especially if the system is delayed. The problems are encountered because the low-pass filter adds a negative-phase shift after the selected cut-off frequency. One other possibility is to apply a simple speed observer

and use the observed signal as a feedback for the proportional part of the PI controller. It is worth noting that this structure resembles the state-space controller structure consisting of a state feedback, a state observer, and an integral state [73].

In the following paragraphs, the two aforementioned methods will be briefly compared as a means of reducing the measurement-noise amplification. Let us first introduce the speed-filtering method, where the measured speed ω_M [see Fig 3.1] is filtered using a first-order low-pass filter:

$$\omega_\mathrm{M,f} = \underbrace{\frac{\alpha_\mathrm{f}}{s+\alpha_\mathrm{f}}}_{G_\mathrm{f}(s)}\omega_\mathrm{M} \tag{3.13}$$

where $\omega_\mathrm{M,f}$ is the filtered motor speed and α_f is the cut-off frequency of the filter. The loop and measurement noise transfer functions of the system with the low-pass filter are given as

$$H_\mathrm{PI,filt}(s) = G(s)C(s)G_\mathrm{t}(s)M(s)G_\mathrm{f}(s) \tag{3.14}$$

$$N_\mathrm{PI,filt}(s) = -C(s)G_\mathrm{t}(s)M(s)G_\mathrm{f}(s) \tag{3.15}$$

respectively. On the other hand, the motor speed can be estimated using a simple single-mass system observer [79]:

$$\frac{d\hat{\omega}_\mathrm{M}}{dt} = \frac{T_\mathrm{M,ref}}{\hat{J}} + l_\mathrm{e}(\omega_\mathrm{M} - \hat{\omega}_\mathrm{M}) \tag{3.16}$$

where $\hat{\omega}_\mathrm{M}$ is the estimated-motor speed, l_e is the observer gain, and $\hat{J}$ is the system-inertia estimate. The observer (3.16) can be given as a transfer function:

$$\hat{\omega}_\mathrm{M} = \frac{1}{\hat{J}(s+l_\mathrm{e})}T_\mathrm{M,ref} + \underbrace{\frac{l_\mathrm{e}}{s+l_\mathrm{e}}}_{G_\mathrm{e}(s)}\omega_\mathrm{M} \tag{3.17}$$

Equations (3.13) and (3.17) show that the same dynamics can be selected for the filter and for the observer if $\alpha_\mathrm{f} = l_\mathrm{e}$. The loop and measurement noise transfer functions of the system with the observer are given as follows:

$$H_\mathrm{PI,est}(s) = k_\mathrm{p}G_\mathrm{e}(s)\left[\frac{1}{\hat{J}l_\mathrm{e}} + G(s)G_\mathrm{t}(s)M(s)\right] + \frac{k_\mathrm{i}}{s}G(s)G_\mathrm{t}(s)M(s) \tag{3.18}$$

$$N_\mathrm{PI,est}(s) = -G_\mathrm{t}(s)M(s)\left[k_\mathrm{p}G_\mathrm{e}(s) + \frac{k_\mathrm{i}}{s}\right] \tag{3.19}$$

respectively.

Fig. 3.2 shows a simulated example from Publication V. In this example, the parameters corresponding to the experimental setup presented in

Section 5.2 are considered and a PI-type speed-feedback controller is applied. The controller is tuned based on (3.4) using $J = 0.02$ kgm^2, $\omega_{\rm d} = 50$ rad/s, and $\zeta_{\rm d} = 0.61$. The speed measurement is accomplished as described in Section 2.7, meaning that the feedback loop delay is $T_{\rm m} + T_{\rm d} = 0.4$ ms, when a sampling period of $h = 0.2$ ms is used. Moreover, the torque-control loop bandwidth $\alpha_{\rm t} = 6$ krad/s is selected and the speed measurement is noisy. To be able to operate despite the noise, both the first-order filter (3.13) and the observer (3.17) are tested when $\alpha_{\rm f} = l_{\rm e} = 10\omega_{\rm d}$ is selected. Fig. 3.2 shows that the high-frequency noise can be suppressed without losing the stability when applying either the low-pass filter or the observer.

Fig. 3.3 shows a simulated case where the feedback-loop time delay is increased to $T_{\rm m} + T_{\rm d} = 2.5$ ms and the undamped natural frequency of the speed-feedback loop is increased to $\omega_{\rm d} = 230$ rad/s. It can be seen that again the high-frequency noise can be suppressed applying either method. However, it is evident from Fig. 3.3(a) that when the first-order filter is applied, the system is very close to being unstable. Thus, applying the the first-order observer would be preferable in this case.

3.2 Two-Mass Systems

The types of feedback controllers, applied for two-mass systems, can be roughly categorized into five groups:

1. PI or PID controller [44, 80–83]

2. PI controller augmented with additional feedbacks [16, 80, 83, 84]

3. PI controller and output filtering [23, 80, 85, 86]

4. state-feedback controller [18, 19, 72, 81]

5. nonlinear control methods, such as sliding-mode [87], neuron-based [84], model-predictive [81], and repetitive-control methods [88]

The main advantage of the PI-type controller is that it allows for straightforward tuning. However, if only the PI controller is applied, then only two of the four closed-loop poles can be freely placed. This is the reason

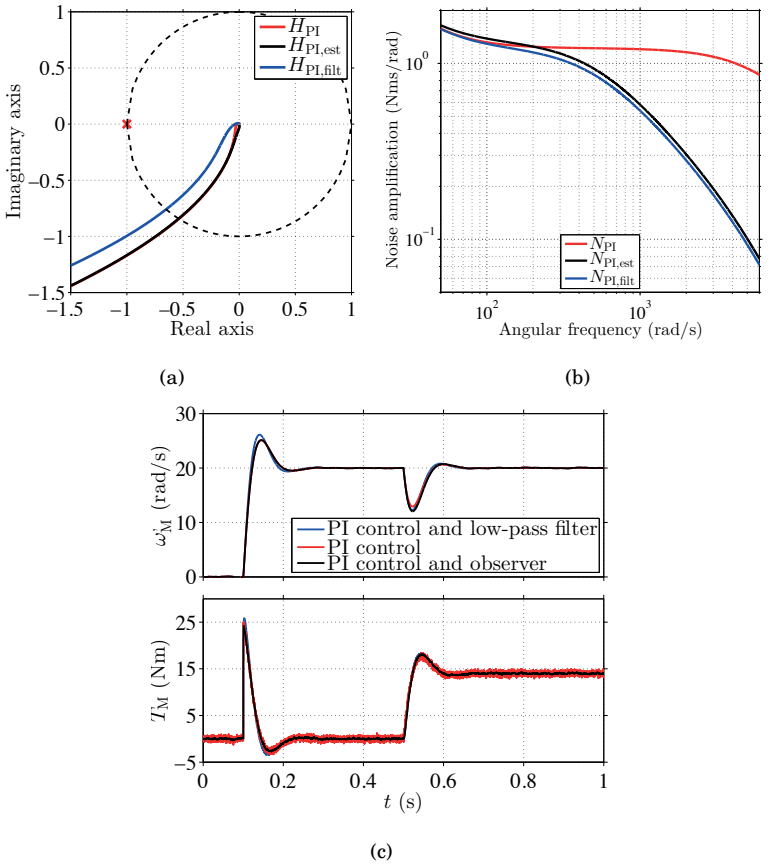

Figure 3.2. Control design example from Publication V: (a) Nyquist curve; (b) noise amplification of the control system; (c) simulated step response and load-torque rejection.

why the PI controller may be augmented with additional feedbacks (e.g., load speed, motor or load acceleration, or estimated load disturbance) or else the controller output may be filtered. On the other hand, if the state-feedback controller is used, then all the closed-loop poles can be freely selected. A drawback of the state-feedback controller is that all the states have to be known.

3.2.1 Feedback Controller Design

This section presents methods to tune a model-based speed controller for a two-mass mechanical system. Both the PI controller and state-space controller tuning are presented. Both controllers are designed in a state-space domain. The speed controller, depicted in Fig. 3.1, is designed in this section under the following assumptions. The estimate of the tor-

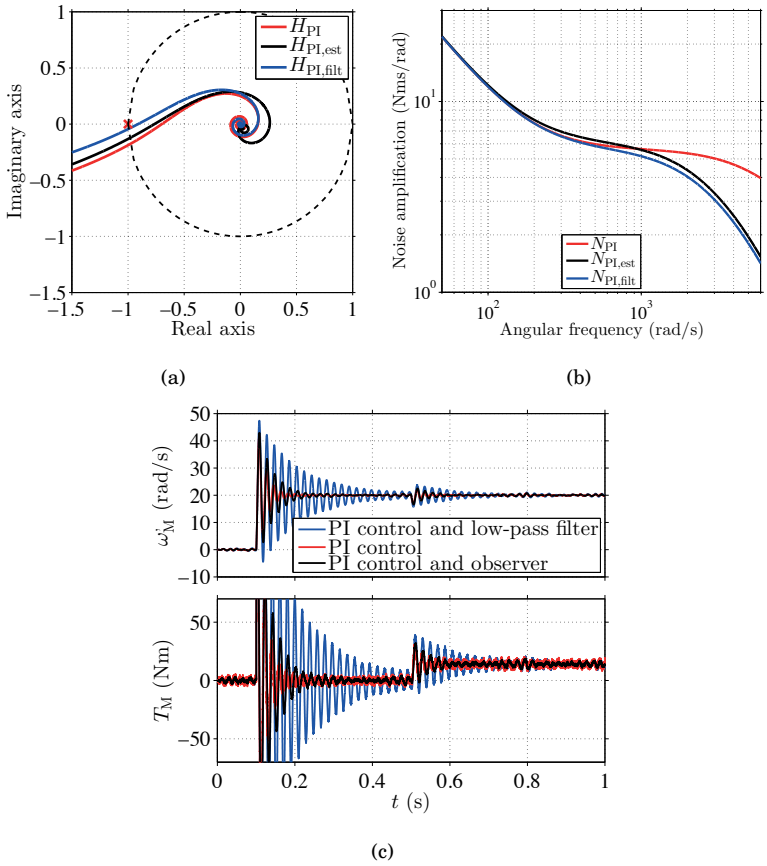

Figure 3.3. Effect of the increased natural damping and feedback-loop time delay ($\omega_{\mathrm{d}} = 230$ rad/s, $T_{\mathrm{d}} + T_{\mathrm{m}} = 2.5$ ms): (a) Nyquist curve; (b) noise amplification of the control system; (c) simulated step response and load-torque rejection.

sional damping is $c_{\mathrm{S}} = 0$; the torque-control loop is ideal and not delayed [$G_{\mathrm{t}}(s) = 1$]; and the speed measurement is ideal and not delayed [$M(s) = 1$]. Furthermore, it is assumed that only the motor speed ω_{M} is available for the feedback controller, but that the load speed ω_{L} is the variable that needs to be controlled. Because the feedback controller should be able to cope with nonzero disturbance torque T_{L}, the state-space model (2.4) should be augmented with the integral state:

$$\dot{x}_{\mathrm{I}} = \omega_{\mathrm{ref,filt}} - \omega_{\mathrm{M}} \tag{3.20}$$

When the PI controller is used, the motor-torque reference is $T_{\mathrm{M}} = k_{\mathrm{p}}\omega_{\mathrm{ref,filt}} - k_{\mathrm{p}}\boldsymbol{C}\boldsymbol{x} + k_{\mathrm{i}}x_{\mathrm{I}}$, where $\boldsymbol{C} = \begin{bmatrix} 1 & 0 & 0 \end{bmatrix}$. When the state-feedback controller is used, the motor-torque reference is $T_{\mathrm{M}} = -\boldsymbol{K}\boldsymbol{x} + k_{\mathrm{i}}x_{\mathrm{I}}$, where $\boldsymbol{K} = \begin{bmatrix} k_1 & k_2 & k_3 \end{bmatrix}$ is the feedback-gain vector. The gain k_{i} is used as the integrator gain in both controller types. For both controllers, the closed-loop

system can be given as

$$\dot{\boldsymbol{x}}_{\mathrm{cl}} = \boldsymbol{A}_{\mathrm{cl}}\boldsymbol{x}_{\mathrm{cl}} + \boldsymbol{B}_{\mathrm{cl,r}}\omega_{\mathrm{ref,filt}} + \boldsymbol{B}_{\mathrm{cl,L}}T_{\mathrm{L}} \tag{3.21}$$

where $\boldsymbol{x}_{\mathrm{cl}} = \begin{bmatrix}\boldsymbol{x}^{\mathrm{T}} & x_{\mathrm{I}}\end{bmatrix}^{\mathrm{T}}$. The eigenvalues (poles) of the closed-loop system can be calculated using the characteristic equation $B(s) = \det(s\boldsymbol{I} - \boldsymbol{A}_{\mathrm{cl}})$. In the following equation, the four poles of $B(s)$ are divided into two pairs of complex poles (dominant and resonant poles):

$$B(s) = \underbrace{(s^2 + 2\zeta_{\mathrm{d}}\omega_{\mathrm{d}}s + \omega_{\mathrm{d}}^2)}_{\text{Dominant poles}}\underbrace{(s^2 + 2\zeta_{\mathrm{r}}\omega_{\mathrm{r}}s + \omega_{\mathrm{r}}^2)}_{\text{Resonant poles}} \tag{3.22}$$

When the feedback loop is closed, the transfer function from $\omega_{\mathrm{ref,filt}}$ to ω_{L} is

$$G_{\mathrm{fb}}(s) = \boldsymbol{C}_{\mathrm{L}}\left(s\boldsymbol{I} - \boldsymbol{A}_{\mathrm{cl}}\right)^{-1}\boldsymbol{B}_{\mathrm{cl,r}} \tag{3.23}$$

and the transfer function from T_{L} to ω_{L} is

$$G_{\mathrm{l}}(s) = \boldsymbol{C}_{\mathrm{L}}\left(s\boldsymbol{I} - \boldsymbol{A}_{\mathrm{cl}}\right)^{-1}\boldsymbol{B}_{\mathrm{cl,L}} \tag{3.24}$$

where $\boldsymbol{C}_{\mathrm{L}} = \begin{bmatrix}0 & 0 & 1 & 0\end{bmatrix}$.

PI Controller

For the PI controller [see (3.1)] the closed-loop system matrices are given as follows:

$$\boldsymbol{A}_{\mathrm{cl}} = \begin{bmatrix}\boldsymbol{A} - \boldsymbol{B}_{\mathrm{u}}k_{\mathrm{p}}\boldsymbol{C} & \boldsymbol{B}_{\mathrm{u}}k_{\mathrm{i}} \\ -\boldsymbol{C} & 0\end{bmatrix} \tag{3.25}$$

$$\boldsymbol{B}_{\mathrm{cl,r}} = \begin{bmatrix}k_{\mathrm{p}}\boldsymbol{B}_{\mathrm{u}} \\ 1\end{bmatrix} \qquad \boldsymbol{B}_{\mathrm{cl,L}} = \begin{bmatrix}\boldsymbol{B}_{\mathrm{w}} \\ 0\end{bmatrix} \tag{3.26}$$

By making $\det(s\boldsymbol{I} - \boldsymbol{A}_{\mathrm{cl}})$ and (3.22) equal to one another, the following is obtained:

$$\begin{aligned}
k_{\mathrm{i}} &= \frac{J_{\mathrm{L}}J_{\mathrm{M}}\omega_{\mathrm{d}}^2\omega_{\mathrm{r}}^2}{K_{\mathrm{S}}} \\
k_{\mathrm{p}} &= 2J_{\mathrm{M}}(\zeta_{\mathrm{d}}\omega_{\mathrm{d}} + \zeta_{\mathrm{r}}\omega_{\mathrm{r}}) \\
0 &= J_{\mathrm{M}}(\omega_{\mathrm{d}}^2 + \omega_{\mathrm{r}}^2 + 4\zeta_{\mathrm{d}}\omega_{\mathrm{d}}\zeta_{\mathrm{r}}\omega_{\mathrm{r}}) - \frac{K_{\mathrm{S}}(J_{\mathrm{M}} + J_{\mathrm{L}})}{J_{\mathrm{L}}} - k_{\mathrm{i}} \\
0 &= \frac{2J_{\mathrm{L}}J_{\mathrm{M}}(\zeta_{\mathrm{d}}\omega_{\mathrm{d}}\omega_{\mathrm{r}}^2 + \zeta_{\mathrm{r}}\omega_{\mathrm{r}}\omega_{\mathrm{d}}^2)}{K_{\mathrm{S}}} - k_{\mathrm{p}}
\end{aligned} \tag{3.27}$$

In the case of the PI controller, two of the four feedback-loop pole coefficients $\{\zeta_{\mathrm{d}}, \omega_{\mathrm{d}}, \zeta_{\mathrm{r}}, \omega_{\mathrm{r}}\}$ can be selected, while the remaining two coefficients together with the controller gains can be found by solving the system of

equations (3.27). As an example, the following symbolic solution can be found if the coefficients of the dominant poles are selected and after that, (3.27) is solved:

$$k_\mathrm{p} = \frac{2J_\mathrm{M}\zeta_\mathrm{d}\omega_\mathrm{d}\left[\frac{K_\mathrm{S}J}{\omega_\mathrm{d}^2 J_\mathrm{M} J_\mathrm{L}} + \frac{J_\mathrm{L}\omega_\mathrm{d}^2}{K_\mathrm{S}} + 2(2\zeta_\mathrm{d}^2 - 1)\right]}{\frac{K_\mathrm{S}}{\omega_\mathrm{d}^2 J_\mathrm{L}} + \frac{J_\mathrm{L}\omega_\mathrm{d}^2}{K_\mathrm{S}} + 2(2\zeta_\mathrm{d}^2 - 1)} \tag{3.28}$$

$$k_\mathrm{i} = \frac{J_\mathrm{M}\omega_\mathrm{d}^2\left(\frac{K_\mathrm{S}J}{\omega_\mathrm{d}^2 J_\mathrm{M} J_\mathrm{L}} + \frac{J_\mathrm{L}\omega_\mathrm{d}^2}{K_\mathrm{S}} - \frac{J}{J_\mathrm{M}} + 4\zeta_\mathrm{d}^2 - 1\right)}{\frac{K_\mathrm{S}}{\omega_\mathrm{d}^2 J_\mathrm{L}} + \frac{J_\mathrm{L}\omega_\mathrm{d}^2}{K_\mathrm{S}} + 2(2\zeta_\mathrm{d}^2 - 1)} \tag{3.29}$$

$$\omega_\mathrm{r} = \sqrt{\frac{k_\mathrm{i} K_\mathrm{S}}{\omega_\mathrm{d}^2 J_\mathrm{M} J_\mathrm{L}}} \tag{3.30}$$

$$\zeta_\mathrm{r} = \frac{k_\mathrm{p}}{2J_\mathrm{M}\omega_\mathrm{r}} - \frac{\zeta_\mathrm{d}\omega_\mathrm{d}}{\omega_\mathrm{r}} \tag{3.31}$$

where $J = J_\mathrm{M} + J_\mathrm{L}$. These PI controller tuning rules were proposed in Publication IV. The closed-loop transfer functions can be calculated using (3.23) and (3.24):

$$G_\mathrm{fb}(s) = \frac{A(s + \frac{k_\mathrm{i}}{k_\mathrm{p}})}{(s^2 + 2\zeta_\mathrm{d}\omega_\mathrm{d}s + \omega_\mathrm{d}^2)(s^2 + 2\zeta_\mathrm{r}\omega_\mathrm{r}s + \omega_\mathrm{r}^2)} \tag{3.32}$$

$$G_\mathrm{l}(s) = -\frac{s\left(\frac{1}{J_\mathrm{L}}s^2 + \frac{k_\mathrm{p}}{J_\mathrm{M}J_\mathrm{L}}s + \frac{k_\mathrm{i}+K_\mathrm{S}}{J_\mathrm{M}J_\mathrm{L}}\right)}{(s^2 + 2\zeta_\mathrm{d}\omega_\mathrm{d}s + \omega_\mathrm{d}^2)(s^2 + 2\zeta_\mathrm{r}\omega_\mathrm{r}s + \omega_\mathrm{r}^2)} \tag{3.33}$$

where $A = \omega_\mathrm{d}^2\omega_\mathrm{r}^2 k_\mathrm{p}/k_\mathrm{i}$.

State-Feedback Controller

For the state-feedback controller, the closed-loop system matrices are as follows:

$$\boldsymbol{A}_\mathrm{cl} = \begin{bmatrix} \boldsymbol{A} - \boldsymbol{B}_\mathrm{u}\boldsymbol{K} & \boldsymbol{B}_\mathrm{u}k_\mathrm{i} \\ -\boldsymbol{C} & 0 \end{bmatrix} \tag{3.34}$$

$$\boldsymbol{B}_\mathrm{cl,r} = \begin{bmatrix} \boldsymbol{0}_{3\times 1} \\ 1 \end{bmatrix} \qquad \boldsymbol{B}_\mathrm{fb,L} = \begin{bmatrix} \boldsymbol{B}_\mathrm{w} \\ 0 \end{bmatrix}$$

The analytical gain selection can be found in Publication VIII.

In the case of the state-feedback controller, the closed-loop poles in (3.22) can be arbitrarily placed by deciding the undamped natural frequencies (ω_d and ω_r) and the damping coefficients (ζ_d and ζ_r). The closed-loop transfer functions can be calculated using (3.23) and (3.24):

$$G_\mathrm{fb}(s) = \frac{\omega_\mathrm{d}^2\omega_\mathrm{r}^2}{(s^2 + 2\zeta_\mathrm{d}\omega_\mathrm{d}s + \omega_\mathrm{d}^2)(s^2 + 2\zeta_\mathrm{r}\omega_\mathrm{r}s + \omega_\mathrm{r}^2)} \tag{3.35}$$

$$G_\mathrm{l}(s) = -\frac{s\left(\frac{1}{J_\mathrm{L}}s^2 + \frac{k_1}{J_\mathrm{M}J_\mathrm{L}}s + \frac{k_2+k_\mathrm{i}+K_\mathrm{S}}{J_\mathrm{M}J_\mathrm{L}}\right)}{(s^2 + 2\zeta_\mathrm{d}\omega_\mathrm{d}s + \omega_\mathrm{d}^2)(s^2 + 2\zeta_\mathrm{r}\omega_\mathrm{r}s + \omega_\mathrm{r}^2)} \tag{3.36}$$

3.2.2 State-Observer Design

When the state-feedback controller is implemented, or if the PI controller is augmented with additional mechanical states (acceleration, loading torque, and so forth), these states have to be known at every time instant. One possibility is to measure the states, meaning that additional sensors are needed. The installed sensors increase the overall cost of the system and may introduce additional uncertainty into the system. Another possibility is to estimate the variables that are needed for the state-feedback controller. This section reviews the basic concepts related to state estimation in two-mass systems. The observers are divided in this section into three groups: full-order observers [89, 90], reduced-order observers [18, 19, 80, 81, 91–93], and disturbance observers [16, 84, 87, 94].

Furthermore, the observer gain selection can be done either by applying a pole placement [16, 18, 80, 81, 84, 87, 89, 91, 94] or by using Kalman-filter techniques [19, 90, 92, 93]. The main difficulty with Kalman-filter techniques is the more-or-less heuristic selection of covariance matrices. These covariance matrices are then needed to calculate the observer gains. Thus, in Publication VIII, the observer gains of both the full-order observer and the reduced-order observer are analytically parametrized in the mechanical parameters and desired observer dynamics. This parametrization makes it possible to apply gain scheduling if needed.

Full-Order Observer

If the states of the system are selected based on (2.4), the full-order state observer can be presented as

$$\dot{\hat{\boldsymbol{x}}} = \underbrace{(\boldsymbol{A} - \boldsymbol{L}\boldsymbol{C})}_{\boldsymbol{A}_\mathrm{o}} \hat{\boldsymbol{x}} + \boldsymbol{B}_\mathrm{u} T_\mathrm{M,ref} + \boldsymbol{L}\omega_\mathrm{M} \tag{3.37}$$

where $\boldsymbol{L} = \begin{bmatrix} l_\mathrm{f1} & l_\mathrm{f2} & l_\mathrm{f3} \end{bmatrix}^\mathrm{T}$ is the full-order observer gain.

Reduced-Order Observer

On the other hand, the reduced-order observer can be presented as follows [73]:

$$\begin{aligned} \dot{\boldsymbol{x}}_\mathrm{r} &= \boldsymbol{A}_\mathrm{r}\hat{\boldsymbol{x}}_\mathrm{ro} + \boldsymbol{B}_\mathrm{r} T_\mathrm{M,ref} + \boldsymbol{B}_\mathrm{y}\omega_\mathrm{M} \\ \hat{\boldsymbol{x}}_\mathrm{ro} &= \boldsymbol{x}_\mathrm{r} + \boldsymbol{L}_\mathrm{r}\omega_\mathrm{M} \end{aligned} \tag{3.38}$$

where $\boldsymbol{L}_\mathrm{r} = \begin{bmatrix} l_\mathrm{r1} & l_\mathrm{r2} \end{bmatrix}^\mathrm{T}$ is the reduced-order observer gain and $\hat{\boldsymbol{x}}_\mathrm{ro} = \begin{bmatrix} \hat{\theta}_\mathrm{M} - \hat{\theta}_\mathrm{L} & \hat{\omega}_\mathrm{L} \end{bmatrix}^\mathrm{T}$. The remaining matrices $\boldsymbol{A}_\mathrm{r}$, $\boldsymbol{B}_\mathrm{r}$, and $\boldsymbol{B}_\mathrm{y}$ can be found

in Publication VIII. Furthermore, Publication VIII demonstrated that the full-order observer is a preferable selection if the feedback loop is delayed and if the speed measurement is noisy.

Disturbance Observer

As an example, a simple rigid-body observer, reported in [16], could be applied to estimate the loading torque. Another possibility is to augment, e.g., the full-order state observer (3.37) with disturbance estimation as follows [18, 92]:

$$\begin{bmatrix} \dot{\hat{\boldsymbol{x}}} \\ \dot{\hat{T}}_{\mathrm{L}} \end{bmatrix} = \begin{bmatrix} \boldsymbol{A}_{\mathrm{o}} & \boldsymbol{B}_{\mathrm{w}} \\ -l_{\mathrm{d}}\boldsymbol{C} & 0 \end{bmatrix} \begin{bmatrix} \hat{\boldsymbol{x}} \\ \hat{T}_{\mathrm{L}} \end{bmatrix} + \begin{bmatrix} \boldsymbol{B}_{\mathrm{u}} \\ 0 \end{bmatrix} T_{\mathrm{M,ref}} + \begin{bmatrix} \boldsymbol{L} \\ l_{\mathrm{d}} \end{bmatrix} \omega_{\mathrm{M}} \tag{3.39}$$

where l_{d} is the disturbance-observer gain. Similarly, the reduced-order observer (3.38) could be augmented with disturbance estimation.

3.2.3 Prefilter or Feedforward Design

As mentioned previously, it is only appropriate to use the feedback controller to stabilize the feedback loop and to reject the loading torques. If the feedback controller is designed for command tracking, the feedback gain increases and stability may be lost. Instead, a feedforward controller (or a prefilter) inserted into the command path can be used to improve the command-tracking capability of the system [22, 72, 78, 95, 96]. A simple acceleration-feedforward technique was introduced for single-mass systems in Section 3.1.2. Because this technique is applied quite often in commercial motion controllers, it is also chosen as a benchmark method for two-mass systems.

The command-tracking dynamics of the system can be designed by selecting first the closed-loop transfer function $\boldsymbol{G}_{\mathrm{c}}(s)$ from the reference vector $\boldsymbol{r}$ to the load speed ω_{L}. Publication IV analytically demonstrated that a zero steady-state tracking error can be obtained for step, ramp, and parabolic commands when selecting the following closed-loop transfer function:

$$\boldsymbol{G}_{\mathrm{c}}(s) = \begin{bmatrix} \alpha & \beta & \gamma \end{bmatrix} \frac{1}{\underbrace{(s^2 + 2\zeta_{\mathrm{l}}\omega_{\mathrm{l}}s + \omega_{\mathrm{l}}^2)}_{\text{Command-tracking poles}} \underbrace{(s^2 + 2\zeta_{\mathrm{r}}\omega_{\mathrm{r}}s + \omega_{\mathrm{r}}^2)}_{\text{Resonant poles}}} \tag{3.40}$$

where $\alpha = \omega_{\mathrm{r}}^2 + \omega_{\mathrm{l}}^2 + 4\zeta_{\mathrm{r}}\zeta_{\mathrm{l}}\omega_{\mathrm{r}}\omega_{\mathrm{l}}$, $\beta = 2(\zeta_{\mathrm{r}}\omega_{\mathrm{r}}\omega_{\mathrm{l}}^2 + \zeta_{\mathrm{l}}\omega_{\mathrm{l}}\omega_{\mathrm{r}}^2)$, and $\gamma = \omega_{\mathrm{r}}^2\omega_{\mathrm{l}}^2$.

The prefilter transfer function $\boldsymbol{F}(s)$ can be solved by making (3.40) and the following equal:

$$\boldsymbol{G}_{\mathrm{c}}(s) = \boldsymbol{F}(s)G_{\mathrm{fb}}(s) \tag{3.41}$$

Likewise, the feedforward-controller transfer function $\boldsymbol{F}_\mathrm{f}(s)$ can be solved by making (3.40) equal to the following:

$$\boldsymbol{G}_\mathrm{c}(s) = \frac{\boldsymbol{F}_\mathrm{f}(s)G_\mathrm{ML}(s) + \begin{bmatrix} 0 & 0 & 1 \end{bmatrix} C(s)G_\mathrm{ML}(s)}{1 + C(s)G_\mathrm{M}(s)} \tag{3.42}$$

As an example, the prefilter transfer functions have been solved for the PI type and for the state-feedback controllers. When the PI-type feedback controller is applied, then the zero and the dominant poles in (3.32) are cancelled out. Thus, the prefilter transfer function from $\boldsymbol{r}$ to $\omega_\mathrm{ref,filt}$ becomes

$$\boldsymbol{F}_\mathrm{PI}(s) = \begin{bmatrix} \alpha & \beta & \gamma \end{bmatrix} \frac{s^2 + 2\zeta_\mathrm{d}\omega_\mathrm{d}s + \omega_\mathrm{d}^2}{A(s + \frac{k_\mathrm{i}}{k_\mathrm{p}})(s^2 + 2\zeta_\mathrm{l}\omega_\mathrm{l}s + \omega_\mathrm{l}^2)} \tag{3.43}$$

On the other hand, when a state-feedback controller is used, only the dominant poles in (3.35) need to be cancelled out and the prefilter transfer function from $\boldsymbol{r}$ to $\omega_\mathrm{ref,filt}$ becomes

$$\boldsymbol{F}_\mathrm{sfb}(s) = \begin{bmatrix} \alpha & \beta & \gamma \end{bmatrix} \frac{s^2 + 2\zeta_\mathrm{d}\omega_\mathrm{d}s + \omega_\mathrm{d}^2}{\omega_\mathrm{d}^2\omega_\mathrm{r}^2(s^2 + 2\zeta_\mathrm{l}\omega_\mathrm{l}s + \omega_\mathrm{l}^2)} \tag{3.44}$$

In both the cases, the natural frequency of the command-tracking dynamics should not be higher than the resonance frequency, meaning that $\omega_\mathrm{l} \leq \omega_\mathrm{r}$.

For implementation purposes, it may be preferable to represent the prefilter transfer function (3.43) or (3.44) as a state-space model:

$$\begin{aligned} \dot{\boldsymbol{x}}_\mathrm{f} &= \boldsymbol{A}_\mathrm{f}\boldsymbol{x}_\mathrm{f} + \boldsymbol{B}_\mathrm{f}\boldsymbol{r} \\ \omega_\mathrm{ref,filt} &= \boldsymbol{C}_\mathrm{f}\boldsymbol{x}_\mathrm{f} + \boldsymbol{D}_\mathrm{f}\boldsymbol{r} \end{aligned} \tag{3.45}$$

As an example, the prefilter matrices for the PI-controlled system (3.43) are as follows:

$$\begin{aligned} \boldsymbol{A}_\mathrm{f} &= \begin{bmatrix} -(\frac{k_\mathrm{i}}{k_\mathrm{p}} + 2\zeta_\mathrm{l}\omega_\mathrm{l}) & -(\frac{2\zeta_\mathrm{l}\omega_\mathrm{l}k_\mathrm{i}}{k_\mathrm{p}} + \omega_\mathrm{l}^2) & -\frac{k_\mathrm{i}\omega_\mathrm{l}^2}{k_\mathrm{p}} \\ 1 & 0 & 0 \\ 0 & 1 & 0 \end{bmatrix} \\ \boldsymbol{B}_\mathrm{f} &= \frac{k_\mathrm{i}}{k_\mathrm{p}} \begin{bmatrix} \frac{1}{\omega_\mathrm{d}^2} + \frac{\omega_\mathrm{l}^2}{\omega_\mathrm{d}^2\omega_\mathrm{r}^2} + \frac{4\zeta_\mathrm{r}\zeta_\mathrm{d}\omega_\mathrm{l}}{\omega_\mathrm{d}^2\omega_\mathrm{r}} & 2\left(\frac{\zeta_\mathrm{r}\omega_\mathrm{l}^2}{\omega_\mathrm{d}^2\omega_\mathrm{r}} + \frac{\zeta_\mathrm{l}\omega_\mathrm{l}}{\omega_\mathrm{d}^2}\right) & \frac{\omega_\mathrm{l}^2}{\omega_\mathrm{d}^2} \\ 0 & 0 & 0 \\ 0 & 0 & 0 \end{bmatrix} \\ \boldsymbol{C}_\mathrm{f} &= \begin{bmatrix} 1 & 2\zeta_\mathrm{d}\omega_\mathrm{d} & \omega_\mathrm{d}^2 \end{bmatrix} \\ \boldsymbol{D}_\mathrm{f} &= \begin{bmatrix} 0 & 0 & 0 \end{bmatrix} \end{aligned} \tag{3.46}$$

The prefilter matrices of the state-feedback controlled system are derived in Publication VIII:

$$\begin{aligned}
\boldsymbol{A}_\mathrm{f} &= \begin{bmatrix} -2\zeta_\mathrm{l}\omega_\mathrm{l} & -\omega_\mathrm{l}^2 \\ 1 & 0 \end{bmatrix} \\
\boldsymbol{B}_\mathrm{f} &= \begin{bmatrix} \frac{1}{\omega_\mathrm{d}^2} + \frac{\omega_\mathrm{l}^2}{\omega_\mathrm{d}^2\omega_\mathrm{r}^2} + \frac{4\zeta_\mathrm{r}\zeta_\mathrm{d}\omega_\mathrm{l}}{\omega_\mathrm{d}^2\omega_\mathrm{r}} & 2\left(\frac{\zeta_\mathrm{r}\omega_\mathrm{l}^2}{\omega_\mathrm{d}^2\omega_\mathrm{r}} + \frac{\zeta_\mathrm{l}\omega_\mathrm{l}}{\omega_\mathrm{d}^2}\right) & \frac{\omega_\mathrm{l}^2}{\omega_\mathrm{d}^2} \\ 0 & 0 & 0 \end{bmatrix} \\
\boldsymbol{C}_\mathrm{f} &= \begin{bmatrix} 2(\zeta_\mathrm{d}\omega_\mathrm{d} - \zeta_\mathrm{l}\omega_\mathrm{l}) & \omega_\mathrm{d}^2 - \omega_\mathrm{l}^2 \end{bmatrix} \\
\boldsymbol{D}_\mathrm{f} &= \begin{bmatrix} \frac{1}{\omega_\mathrm{d}^2} + \frac{\omega_\mathrm{l}^2}{\omega_\mathrm{d}^2\omega_\mathrm{r}^2} + \frac{4\zeta_\mathrm{r}\zeta_\mathrm{d}\omega_\mathrm{l}}{\omega_\mathrm{d}^2\omega_\mathrm{r}} & 2\left(\frac{\zeta_\mathrm{r}\omega_\mathrm{l}^2}{\omega_\mathrm{d}^2\omega_\mathrm{r}} + \frac{\zeta_\mathrm{l}\omega_\mathrm{l}}{\omega_\mathrm{d}^2}\right) & \frac{\omega_\mathrm{l}^2}{\omega_\mathrm{d}^2} \end{bmatrix}
\end{aligned} \tag{3.47}$$

3.3 Discrete-Time Implementation

Regardless of whether the PI controller or the state-space controller is applied, the speed controller can be presented in a generalized matrix form as follows:

$$\begin{aligned}
\dot{\boldsymbol{x}}_\mathrm{c} &= \boldsymbol{A}_\mathrm{c}\boldsymbol{x}_\mathrm{c} + \boldsymbol{B}_\mathrm{c}\boldsymbol{u}_\mathrm{c} \\
T_\mathrm{c} &= \boldsymbol{C}_\mathrm{c}\boldsymbol{x}_\mathrm{c} + \boldsymbol{D}_\mathrm{c}\boldsymbol{u}_\mathrm{c}
\end{aligned} \tag{3.48}$$

where $\boldsymbol{u}_\mathrm{c} = \begin{bmatrix} \boldsymbol{r}^\mathrm{T} & \omega_\mathrm{M} & T_\mathrm{c,sat} - T_\mathrm{c} \end{bmatrix}^\mathrm{T}$ is the controller input vector and T_c is the controller output. The saturated controller output $T_\mathrm{c,sat}$ is

$$T_\mathrm{c,sat} = \begin{cases} T_\mathrm{c}, & \text{if } |T_\mathrm{c}| \leq T_\mathrm{c,max} \\ T_\mathrm{c,max}\mathrm{sgn}(T_\mathrm{c}), & \text{if } |T_\mathrm{c}| > T_\mathrm{c,max} \end{cases} \tag{3.49}$$

where $T_\mathrm{c,max}$ is the maximum torque and $\mathrm{sgn}(\cdot)$ the signum function. The closed-loop system matrices $\boldsymbol{A}_\mathrm{c}$, $\boldsymbol{B}_\mathrm{c}$ $\boldsymbol{C}_\mathrm{c}$, $\boldsymbol{D}_\mathrm{c}$ and the controller state-vector $\boldsymbol{x}_\mathrm{c}$ depend on the selected linear speed-control method.

When the 2DOF PI controller for the two-mass system is applied and the integrator (3.20) is equipped with an anti-reset windup (i.e., $\dot{x}_\mathrm{I} = \omega_\mathrm{ref,filt} - \omega_\mathrm{M} + [T_\mathrm{c,sat} - T_\mathrm{c}]/k_\mathrm{p}$), then the controller states can be selected as $\boldsymbol{x}_\mathrm{c} = \begin{bmatrix} x_\mathrm{I} & \boldsymbol{x}_\mathrm{f}^\mathrm{T} \end{bmatrix}^\mathrm{T}$ and, thus, the closed-loop matrices become

$$\begin{aligned}
\boldsymbol{A}_\mathrm{c} &= \begin{bmatrix} 0 & \boldsymbol{C}_\mathrm{f} \\ \boldsymbol{0}_{3\times1} & \boldsymbol{A}_\mathrm{f} \end{bmatrix} \qquad \boldsymbol{B}_\mathrm{c} = \begin{bmatrix} \boldsymbol{D}_\mathrm{f} & -1 & 1/k_\mathrm{p} \\ \boldsymbol{B}_\mathrm{f} & \boldsymbol{0}_{3\times1} & \boldsymbol{0}_{3\times1} \end{bmatrix} \\
\boldsymbol{C}_\mathrm{c} &= \begin{bmatrix} k_\mathrm{i} & k_\mathrm{p}\boldsymbol{C}_\mathrm{f} \end{bmatrix} \qquad \boldsymbol{D}_\mathrm{c} = \begin{bmatrix} k_\mathrm{p}\boldsymbol{D}_\mathrm{f} & -k_\mathrm{p} & 0 \end{bmatrix}
\end{aligned} \tag{3.50}$$

The aforementioned controller can be converted into a discrete-time, state-space representation:

$$\begin{aligned}
\boldsymbol{x}_\mathrm{c}(k+1) &= \boldsymbol{\Phi}_\mathrm{c}\boldsymbol{x}_\mathrm{c}(k) + \boldsymbol{\Gamma}_\mathrm{c}\boldsymbol{u}_\mathrm{c}(k) \\
T_\mathrm{c}(k+1) &= \boldsymbol{H}_\mathrm{c}\boldsymbol{x}_\mathrm{c}(k) + \boldsymbol{J}_\mathrm{c}\boldsymbol{u}_\mathrm{c}(k)
\end{aligned} \tag{3.51}$$

where the discrete-time system matrices can be formed by applying, for example, Tustin's bilinear transformation [97]:

$$\begin{aligned}
\boldsymbol{\Phi}_\mathrm{c} &= (\boldsymbol{I} + \boldsymbol{A}_\mathrm{c}h/2)(\boldsymbol{I} - \boldsymbol{A}_\mathrm{c}h/2)^{-1} \\
\boldsymbol{\Gamma}_\mathrm{c} &= (\boldsymbol{I} - \boldsymbol{A}_\mathrm{c}h/2)^{-1}\boldsymbol{B}_\mathrm{c}\sqrt{h} \\
\boldsymbol{H}_\mathrm{c} &= \sqrt{h}\boldsymbol{C}_\mathrm{c}(\boldsymbol{I} - \boldsymbol{A}_\mathrm{c}h/2)^{-1} \\
\boldsymbol{J}_\mathrm{c} &= \boldsymbol{C}_\mathrm{c}(\boldsymbol{I} - \boldsymbol{A}_\mathrm{c}h/2)^{-1}\boldsymbol{B}_\mathrm{c}h/2
\end{aligned} \tag{3.52}$$

It is worth noting that the 2DOF controller for single-mass systems, presented in Section 3.1 and in Publication V, can also be recast as similar presentation. Furthermore, the discrete-time implementation of the state-space controller is given in the Appendix of Publication VIII.

3.4 Robustness and Measurement-Noise Amplification

Publication VIII demonstrated that the state-space controller can be applied without difficulties using either the full-order observer or the reduced-order observer, even if the feedback loop is delayed. However, the study also showed that the full-order observer clearly suppresses the high-frequency noise better than the reduced-order observer, meaning that it is a preferable option if the speed measurement is noisy. Furthermore, a comparison of the measurement-noise sensitivity and the sensitivity to the torque-control loop dynamics was carried out for the state-space controller and the PI controller. Nyquist diagrams, noise transfer functions, time-domain simulations, and experimental results were used to demonstrate that the full-order-observer based controller outperforms the PI controller if the feedback loop is delayed and noisy. As an example, Fig. 3.4 shows the feedback-loop characteristics of both the PI controller and the state-space controller. Furthermore, if the feedback loop is both delayed and fast ($\omega_\mathrm{d} > \omega_\mathrm{ares}$), the inertia ratio $R = J_\mathrm{L}/J_\mathrm{M}$ affects the selection of the resonant-pole coefficients $\{\zeta_\mathrm{r}, \omega_\mathrm{r}\}$. The loop transfer functions and the noise transfer functions of the different controller types can be found in Publication VIII.

In addition to the results presented in Publication VIII, this paragraph compares three different model-based, PI-controller pole-placement techniques. Reference [83] has proposed placing the four feedback-loop poles as a double complex-conjugate pole pair. If just the PI controller is applied, the location of this double-pole pair cannot be decided. Instead, it depends on the mechanical parameters of the system. Reference [82] pro-

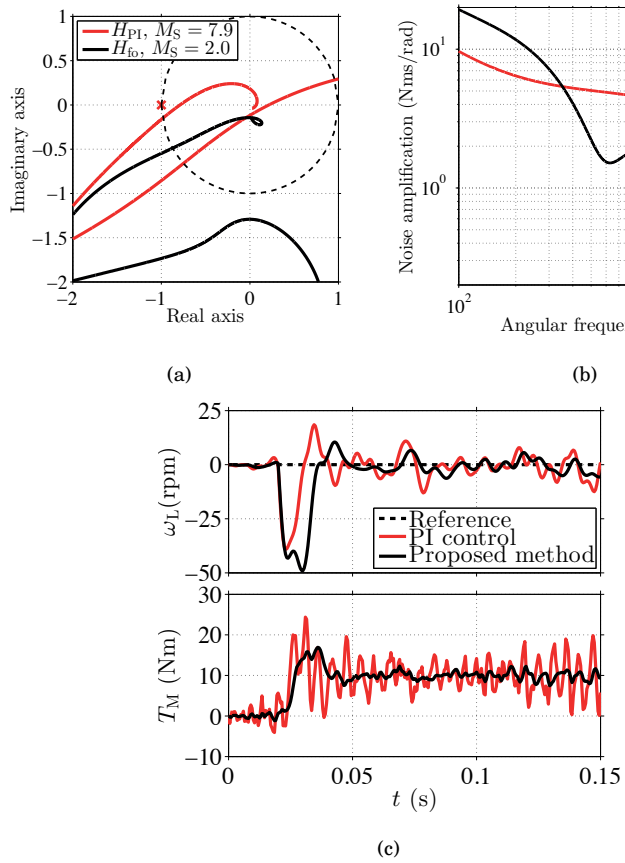

Figure 3.4. Feedback-loop characteristics: (a) Nyquist curve; (b) noise amplification of the control system; (c) simulated load-torque rejection. The sensitivity-function peak is indicated as M_S (see Publication VIII for further details).

pose using a more elaborate scheme, one in which the parameters of the feedback controller are used to select certain coefficients (natural frequencies or dampings) from both the dominant and resonant poles. However, as discussed in Publication IV, it is preferable to place the dominant and resonant poles into separate regions in the s-plane, because in that case, the lower-frequency poles decide more clearly the dominant dynamics of the closed loop. It should be noted that, if only the PI controller is applied and the feedback is the motor's angular speed, then the antiresonance frequency limits the selection of the dominant poles, that is to say $\omega_d \leq \omega_{ares}$. Fig. 3.5 shows the three pole-placement techniques being compared in this section. The mechanical parameters used in this example are listed in Table 5.2. The feedback-loop pole coefficients for this parameter set are shown in Table 3.1. Furthermore, the feedback loop is delayed (see Publication VIII, Section IV-A).

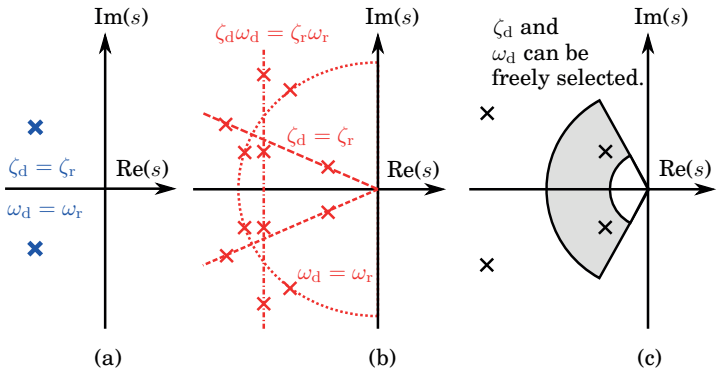

Figure 3.5. PI-controller pole-placement techniques: (a) Double complex-conjugate poles [83]; (b) identical damping coefficients (marked as dashed line), an identical real part (marked as dash-dotted line), and an identical radius (marked as dotted line) [82]; (c) arbitrary selection of dominant poles (see Publication IV).

Fig. 3.6(a) shows the Nyquist diagrams of the loop transfer functions and the measurement-noise amplifications of the three PI-controller pole placements. According to the Nyquist diagrams, all of the tuning methods give a stable feedback-loop operation. However, the distance between the critical point and the loop transfer function curve is clearly longest for the proposed pole selection, meaning that it is a more robust option. According to the measurement-noise amplification, shown in Fig. 3.6(b), similar conclusions can be made. Fig. 3.6(c) shows that the time-domain simulation results for the load-torque rejection agree well with the frequency-domain analysis.

It is worth noting that the PI control techniques could be augmented with, for example, the single-mass system observer to reduce the measurement-noise amplification, similarly as in Section 3.1.3. However, the sensitivity to the delayed-feedback loop should be checked after com-

Table 3.1. Feedback-loop pole coefficients $\{\zeta_\mathrm{d},\, \omega_\mathrm{d},\, \zeta_\mathrm{r},\, \omega_\mathrm{r}\}$ for different assignment techniques and command-tracking pole coefficients $\{\zeta_\mathrm{l},\, \omega_\mathrm{l}\}$ for the proposed 2DOF controller (The magenta-marked values can be selected freely)

	Proposed	In [83]	In [82]
ζ_d	0.8	$\sqrt{R}/2$	0.6
ω_d	$\omega_\mathrm{ares}/2$	ω_ares	$\omega_\mathrm{ares}\sqrt{2(1-2\zeta_\mathrm{d}^2)}$
ζ_r	Eq. (3.31)	$\sqrt{R}/2$	$\sqrt{1/2-\zeta_\mathrm{d}^2}$
ω_r	Eq. (3.30)	ω_ares	$2\zeta_\mathrm{d}\omega_\mathrm{ares}$
ζ_l	1	—	—
ω_l	$(2\omega_\mathrm{ares}+\omega_\mathrm{res})/3$	—	—

pleting the observer design.

3.5 Input-Command Shaping and Tracking Error

The residual vibrations appearing in the two- or multi-mass systems may be suppressed by applying the feedback controller, as was discussed in Section 3.2. On the other hand, input-command shaping offers another possibility for suppressing vibrations and some of the techniques are introduced in this section.

Furthermore, several papers describe how to tackle the problems of implementing these input profiles online. This section provides a brief review of the input-command-shaping techniques and the problems associated with them. The techniques, reported in the literature, may be divided

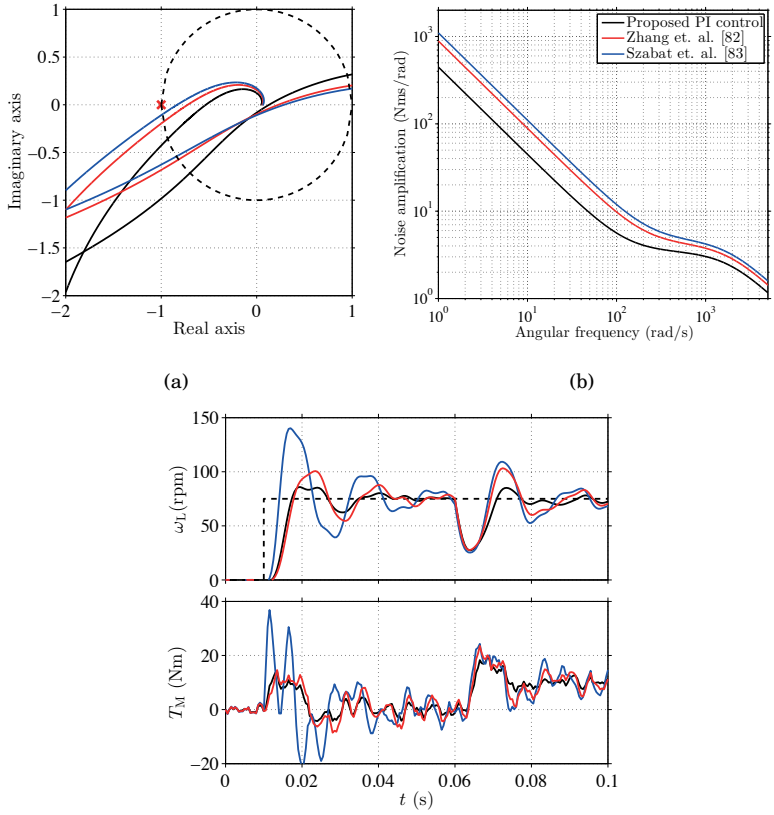

Figure 3.6. Feedback-loop characteristics of the different PI-controller pole placements: (a) Nyquist curve; (b) noise amplification of the control system; (c) simulated step response and load-torque rejection.

into two major categories:

1. Model-based techniques, for example [9, 98–100]

2. Direct methods, for example [101–103]

The model-based methods use the knowledge of the controlled plant, and the input profile is generated so that the frequencies around the resonance frequency are attenuated. This can be done by introducing filters [9, 99], or by manipulating the acceleration/deceleration and jerk up/down times of an s-shaped motion profile [98, 100].

Also, the direct methods apply stepwise-jerk profiles, higher-order polynomial profiles [101, 102], or trigonometric profiles [103]. It is stated in [102] that the jerk profile should be as smooth as possible so as not to excite the mechanical vibrations of the controlled system. Thus, the applicability of the stepwise-jerk profiles may be limited, if the residual vibrations are not attenuated by the feedback controller.

The development of the input-command-shaping techniques is outside the scope of this dissertation. However, because the prefiltering topic was covered in the 2DOF control design (Section 3.1.2 for the single-mass systems and Section 3.2.3 for the two-mass systems), the tracking of different references is briefly studied here. The command-tracking tests were done for a 2DOF PI-controlled two-mass system (with mechanical parameters listed in Table 5.3). The control-design parameters were as follows: $\omega_\mathrm{d} = \omega_\mathrm{ares}/2$, $\zeta_\mathrm{d} = 0.8$, $\omega_\mathrm{l} = \omega_\mathrm{res}$, and $\zeta_\mathrm{l} = 1$, where ω_ares and ω_res are calculated according to (2.8). Furthermore, the feedback loop is delayed and the total time delay is $T_\mathrm{m} + T_\mathrm{d} = 0.7$ ms when a sampling period of $h = 0.5$ ms is used. A torque-control loop bandwidth of $\alpha_\mathrm{t} = 1.8$ krad/s was selected.

The tested input commands are shown in Figs. 3.7(a) and 3.7(b). All of the commands were designed so that the angular position of the load θ_L rotates 10 revolutions in 2 seconds. Fig. 3.7(a) shows a stepwise speed reference and a triangle (i.e., acceleration-bounded) speed reference. Fig. 3.7(b) shows different jerk-bounded speed references and Fig. 3.7(c) shows the jerk profiles associated with these references. The results were compared for the proposed PI-type feedback controller in three cases: 1) When just the feedback controller is applied, that is, when $\boldsymbol{F}(s) = \begin{bmatrix} 0 & 0 & 1 \end{bmatrix}$ (referred to as a 1DOF controller); 2) when the feedback controller is augmented with the acceleration feedforward (3.12) (referred to as an acceleration

feedforward 1DOF controller); 3) when the feedback controller is applied together with the prefilter (3.43) (referred to as a 2DOF controller).

Fig. 3.8 shows command-tracking errors for the three cases when the triangle-speed reference is used. Figs. 3.8(b) and 3.8(c) show that nearly identical command-tracking errors are obtained when using the proposed 2DOF controller and the acceleration feedforward 1DOF controller. Fig. 3.8(a) shows that the tracking error of the 1DOF controller is clearly the highest.

Fig. 3.9 shows command-tracking errors for the three cases when the polynomial-speed references are used. When comparing Figs. 3.9(b) and 3.9(c), it is evident that the proposed 2DOF controller clearly outperforms the acceleration feedforward 1DOF controller. Fig. 3.9(a) shows that the tracking error of the 1DOF controller is clearly the highest.

Fig. 3.10 shows command-tracking errors for the three cases when the trigonometric references are used. When comparing Figs. 3.10(b) and 3.10(c), it is once again evident that the proposed 2DOF controller clearly outperforms the acceleration feedforward 1DOF controller. Fig. 3.10(a) shows that again, the tracking error of the 1DOF controller is clearly the highest.

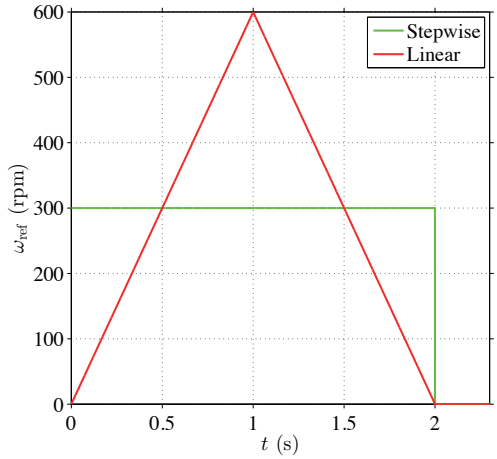

(a)

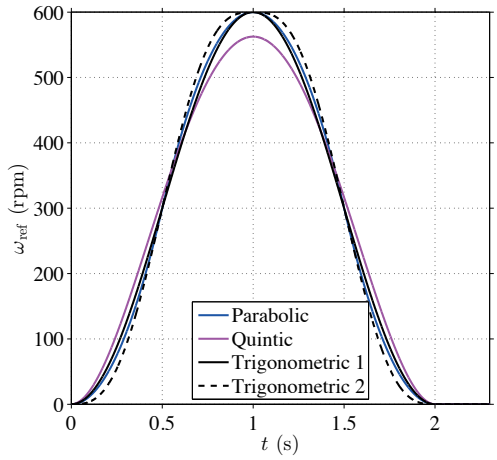

(b)

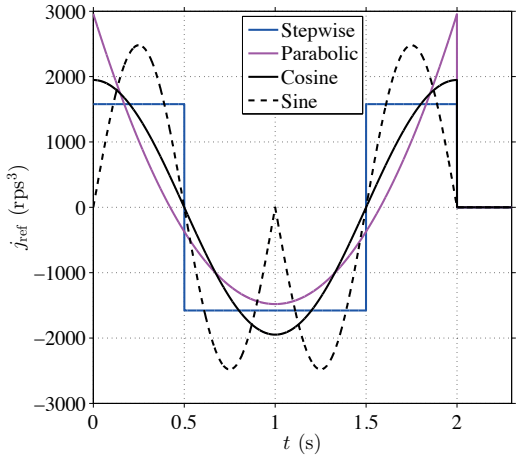

(c)

Figure 3.7. Reference trajectories: (a) Step reference and acceleration-bounded reference (triangle/trapezoidal reference); (b) jerk-bounded references; (c) jerk profiles.

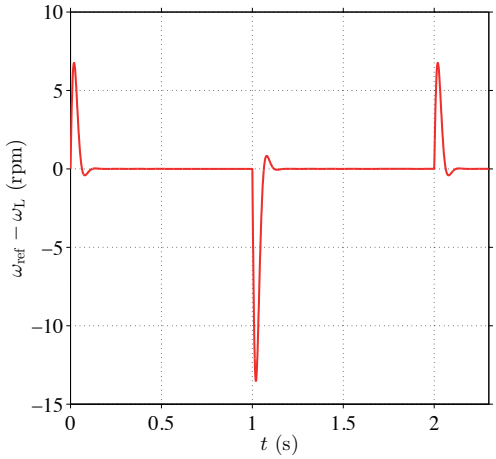

(a)

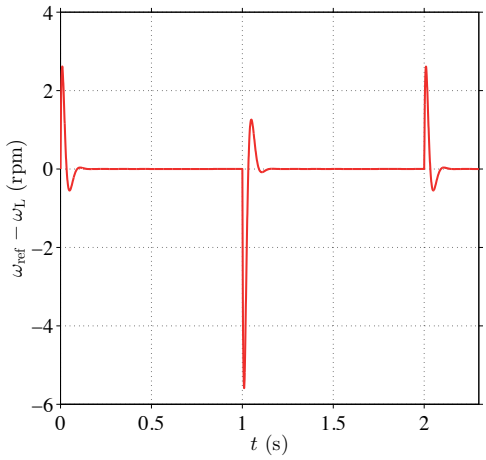

(b)

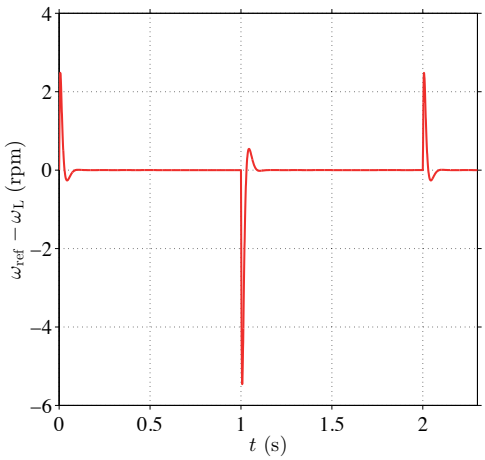

(c)

Figure 3.8. Command-tracking error for triangle reference when applying (a) a 1DOF controller; (b) an acceleration feedforward 1DOF controller; and (c) a 2DOF controller.

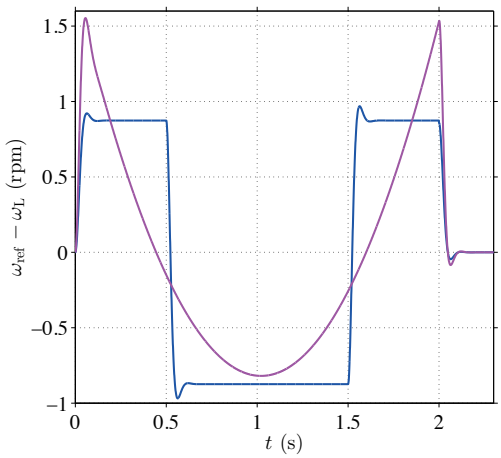

(a)

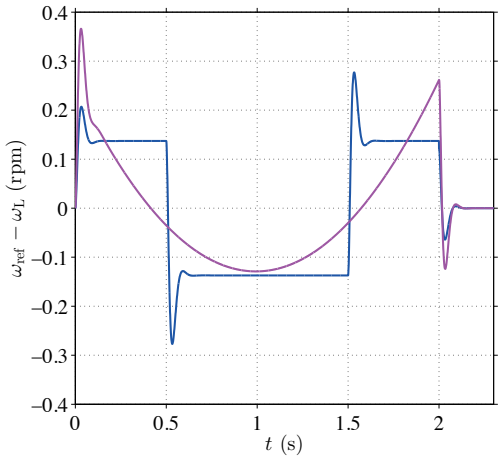

(b)

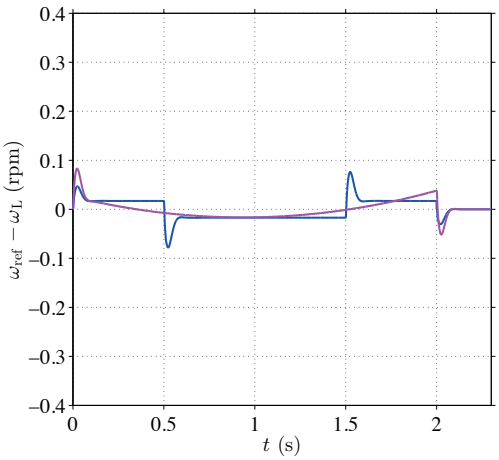

(c)

Figure 3.9. Command-tracking error for polynomial references when applying (a) a 1DOF controller; (b) an acceleration feedforward 1DOF controller; and (c) a 2DOF controller.

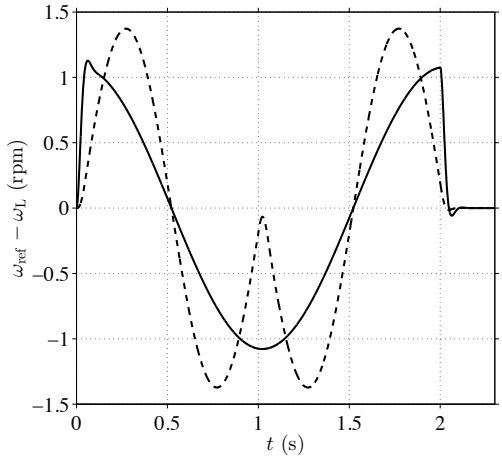

(a)

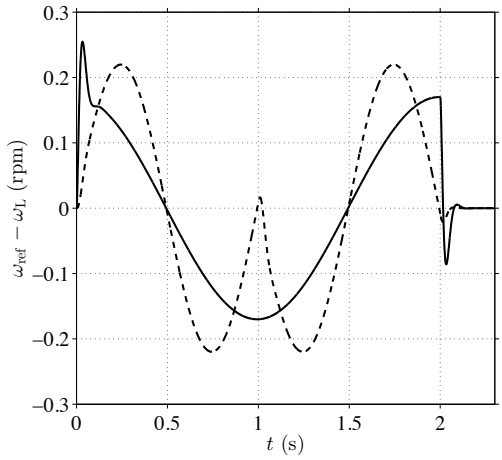

(b)

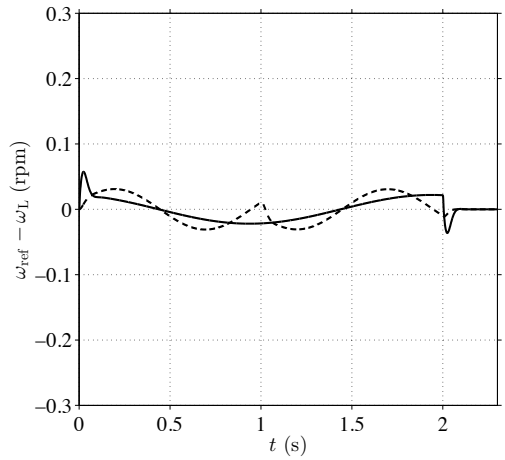

(c)

Figure 3.10. Command-tracking error for trigonometric references when applying (a) a 1DOF controller; (b) an acceleration feedforward 1DOF controller; and (c) a 2DOF controller.

4. Identification

As discussed in Chapter 3, tuning the speed or position controller typically relies on knowledge of mechanical parameters and some performance specifications (e.g., closed-loop bandwidth). However, datasheets of the mechanical components are not often available or else calculating the mechanical parameters can be a highly complex task. This was pointed out in Chapter 2. Hence, to enable model-based automatic tuning of the motion controllers, the mechanical parameters should be automatically identified when starting up a drive [91] or else when normally operating the drive [104, 105].

This chapter reviews typical methods for identifying the mechanical systems in electric drives. There are two major types of identification routines: Nonparametric estimation methods [27, 29, 106–108] and parametric estimation methods [8, 30, 91, 104]. Moreover, both of these methods may be applied when the system operates in an open-loop mode or when a closed-loop speed or position control is used. Fig. 4.1 shows a generalized setup, which can be applied to identify mechanical loads in electric drives.

The excitation signal u should contain all frequencies evenly distributed, and the variance of the excitation signal should be as large as possible. White noise is normally utilized for stochastical identification. In electric drives, the torque and the speed are limited to their maximum allowed values. With limited input signals, the largest variance is obtained by binary signals, which have only two possible values (e.g., -1 and 1). A pseudo-random binary signal (PRBS) fulfills the previously stated requirements, and it can easily be generated using a shift register. The statistical properties of the PRBS have been studied in [109].

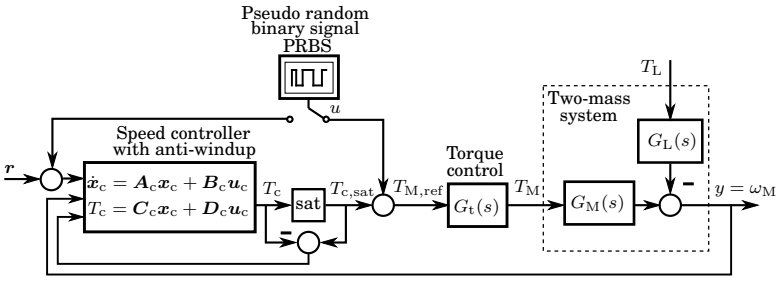

Figure 4.1. Identification setup.

4.1 Nonparametric Methods

Nonparametric methods use the frequency-domain characteristics of the system [26]. As an example, in [106], a transfer function is identified in the frequency domain without any prior knowledge of the resonance characteristics and time delay of the system. Furthermore, a nonparametric identification may be done by using a step response of the system in the continuous-time domain or in the discrete-time domain. It is evident that if frequency-response based methods are applied, the measured data will need to be available in the frequency domain. However, the measured signals are usually collected as a time series, meaning that the time-domain data must first be converted into the frequency domain using some specified algorithm. This conversion process always results in an extra calculation and the accuracy of the calculation depends on the conversion method [27]. Moreover, if the physical parameters of the system are of interest, an additional parameter-fitting algorithm is always needed when nonparametric methods are applied. The need for a parameter-fitting algorithm further increases the calculation burden when doing this type of identification.

Because of these drawbacks, nonparametric methods are only applied for benchmark comparisons in Publication VII during the course of this dissertation.

4.2 Polynomial-Model Based Methods

With polynomial-model based (i.e., parametric) methods, the parameters of the transfer-function polynomials are estimated in either the discrete-time domain or in the continuous-time domain. The problem with continuous-time estimation methods often has to do with the need to find

derivatives for the variables. Calculating the derivatives from measured signals introduces additional noise, which adds a certain amount of bias into the parameter estimates. However, it is possible to integrate both sides of a differential equation model in order to obtain a derivative-free equation [110]. However, the integration process has to be completed using some numerical method, which may induce inaccuracies. In [91], the mechanical parameters were estimated in a continuous-time domain using an evolutionary-based algorithm.

4.2.1 Selection of the Model Structure

When the parametric estimation method is applied, it is important to select the structure and the degree of the polynomial model correctly. If the model structure is known beforehand, the degree of the model can be selected directly. This was assumed in Publication III, Publication VI, and Publication VII. On the other hand, if the model structure is unknown, stochastical properties of the residuals can be used to iteratively search for the appropriate degree for the model [111].

Three different model structures (OE, ARX, and ARMAX) were tested in an open-loop identification configuration in Publication III and it was discovered that the OE structure is an appropriate selection. The same observation has also been made in [8, 31]. Furthermore, as discussed in Section 2.7, the main source of noise in the electric drive system results from the quantization of the position and speed signals. This also justifies the selection of the OE-model structure.

4.2.2 Open-Loop Identification

Fig. 4.1 shows a setup for identifying mechanical loads in electric drives. The open-loop transfer function can be directly estimated based on the excitation signal u and the measured output signal y, when T_c is set to zero. However, if the excitation signal has a zero average, identification will be performed in the vicinity of zero speed. In this case, the friction phenomena are highly nonlinear and can cause bias in the parameter estimates. It is desirable to reduce the effect of the nonlinear friction phenomena on the parameter estimates by operating at nonzero speed. However, when using the open-loop method, it may be difficult to find a suitable value for the offset torque without causing the system to rush. Open-loop identification has been studied, for example, in [27, 112]. Furthermore, it has

Table 4.1. Discrete-time polynomials needed for parameter estimation

	single-mass system	two-mass system
$B_{\mathrm{M,d}}(z)$	θ_1	$\theta_1 z^2 + \theta_2 z + \theta_3$
$A_{\mathrm{d}}(z)$	$z + \theta_2$	$z^3 + \theta_4 z^2 + \theta_5 z + \theta_6$
$B_{\mathrm{L,d}}(z)$	θ_1	$\theta_7 z + \theta_8$
$G_{\mathrm{t}}(z)$	1	1 or $\frac{1+\theta_{\mathrm{t}}}{z+\theta_{\mathrm{t}}}$
$A_{\mathrm{f}}(z)$	$z + \theta_2$	$A_{\mathrm{d}}(z)$ or $A_{\mathrm{d}}(z)(z + \theta_{\mathrm{t}})$
$u(k)$	Excitation PRBS	Excitation PRBS
$T_{\mathrm{M,ref}}(k)$	Eq. (4.2), Eq. (4.3) or $u(k)$	Eq. (4.2), Eq. (4.3) or $u(k)$
$T_{\mathrm{L}}(k)$	known or estimated	known or estimated
Mechanical parameters	$b = \frac{1+\theta_2}{\theta_1}$ $J = \frac{-bh}{\ln(-\theta_2)}$	Section 4.2.5

been applied in Publication III and in Publication VII.

4.2.3 Closed-Loop Identification

When applying closed-loop identification, the drive can easily be operated at the desired (nonzero) speed. Closed-loop identification methods can be divided into direct and indirect methods [113]. In the case of direct methods, the input signal is affected via the feedback loop. Hence, the correct noise model is needed. In the case of indirect methods, the closed-loop system is first identified, and the the open-loop model is solved using the known control law. For the most part, the direct closed-loop estimation method has been applied in this context this far (e.g., [8, 27, 91]). With the direct method, the effect of the feedback controller is omitted and the open-loop transfer function parameters are estimated directly [113]. If the effect of the speed controller is omitted, the higher the feedback controller gain, the more biased the parameter estimates [30]. Another possibility is to estimate the closed-loop transfer function. However, finding analytical relationships for the mechanical parameter estimates would become more complicated because the order of the transfer function increases. Publication VI proposes a method to identify two-mass mechanical system in closed-loop speed control.

4.2.4 Iterative Output-Error Estimation

According to Fig. 4.1, the output y of the system is

$$y(k) = \frac{B_{\mathrm{M,d}}(z)}{A_{\mathrm{d}}(z)} G_{\mathrm{t}}(z) T_{\mathrm{M,ref}}(k) - \frac{B_{\mathrm{L,d}}(z)}{A_{\mathrm{d}}(z)} T_{\mathrm{L}}(k) + e(k) \tag{4.1}$$

where z is the time-shift operator, and $y(k) = \omega_{\mathrm{M}}(k)$, $T_{\mathrm{M,ref}}(k)$, and $T_{\mathrm{L}}(k)$ are the discrete samples corresponding to the signals $y = \omega_{\mathrm{M}}$, $T_{\mathrm{M,ref}}$, and T_{L}, respectively. The time index of the discretized signals is k and the output noise is $e(k)$.

The numerator $B_{\mathrm{M,d}}(z)$ and the denominator $A_{\mathrm{d}}(z)$ in (4.1) depend on the transfer function to be identified. These can refer, for example, to the zero-pole equivalent discretizations of the single-mass system transfer function (2.2) or to the two-mass system transfer function (2.5). The load-transfer function $B_{\mathrm{L,d}}(z)/A_{\mathrm{d}}(z)$ is needed only if the system is loaded during the identification. Furthermore, the torque-control loop dynamics can be assumed to be ideal [i.e., $G_{\mathrm{t}}(z) = 1$] if the torque-control loop is fast, cf. Section 2.5. More information about selecting the discrete-time polynomials can be found in Table 4.1, in Publication VI, and in Publication VII.

In order to obtain all the necessary signals for the identification [see (4.1)], the torques $T_{\mathrm{M,ref}}(k)$ and $T_{\mathrm{L}}(k)$ need to be defined first. It can be assumed that the reference vector $\boldsymbol{r}(k)$, the excitation PRBS $u(k)$, and the measured motor speed $y(k)$ are the known signals. Furthermore, the excitation signal $u(k)$ can be injected either into the reference vector or into the output of the speed controller. If the excitation signal is added to the output of the speed controller, the motor torque reference is as follows:

$$T_{\mathrm{M,ref}}(k) = u(k) + T_{\mathrm{c,sat}}(k) \tag{4.2}$$

On the other hand, if the excitation signal is added to the speed-controller reference, the motor torque reference is

$$T_{\mathrm{M,ref}}(k) = T_{\mathrm{c,sat}}(k) \tag{4.3}$$

The saturated speed controller output is calculated using (3.49), where the contribution of the of the 2DOF speed controller $T_{\mathrm{c}}(k)$ can be calculated using (3.51) and (3.52), when the applied control method is known. If the loading cycle of the drive system is known a priori, it can be used to define the loading torque T_{L} needed for the parameter estimation. Another possibility is to estimate the loading torque using, for example, a disturbance observer.

The output of the pulse-transfer function (4.1) can be expressed as

$$y(k) = \boldsymbol{\phi}^{\mathrm{T}}(k)\boldsymbol{\theta} \tag{4.4}$$

where the predictor vector ϕ and the parameter vector $\boldsymbol{\theta}$ depend on the identification configuration. When the noise component is added to the output of the system, solving the parameter vector using (4.4) leads to biased parameter estimates [26]. Here, a straightforward iterative method is applied to reduce the bias in the parameter estimates [111]. With this method, the input and output signals are filtered using the closed-loop system denominator polynomial $A_{\mathrm{f}}(z)$ from the previous iteration. The output of the adaptive filtered system is given as

$$y_{\mathrm{f}}(k) = \boldsymbol{\phi}_{\mathrm{f}}^{\mathrm{T}}(k)\boldsymbol{\theta} \tag{4.5}$$

where the filtered predictor vector and output are

$$\boldsymbol{\phi}_{\mathrm{f}}(k) = \frac{1}{A_{\mathrm{f}}(z)}\boldsymbol{\phi}(k) \qquad y_{\mathrm{f}}(k) = \frac{1}{A_{\mathrm{f}}(z)}y(k) \tag{4.6}$$

respectively. The filtering polynomial can be selected as $A_{\mathrm{f}}(z) = A_{\mathrm{d}}(z)$ if an ideal torque-control loop is assumed. On the other hand, $A_{\mathrm{f}}(z) = A_{\mathrm{d}}(z)(z + \theta_{\mathrm{t}})$ is selected if the torque-control loop dynamics are included in parameter estimation (see Publication VI). When estimating the parameter vector $\boldsymbol{\theta}$, the observations are packed into the adaptive-filtered output vector $\boldsymbol{y}_{\mathrm{f}}$ and predictor matrix $\boldsymbol{\Phi}_{\mathrm{f}}$. Then, these matrices are used in an iterative least-squares algorithm to solve the parameter vector:

$$\boldsymbol{\theta} = \left(\boldsymbol{\Phi}_{\mathrm{f}}^{\mathrm{T}}\boldsymbol{\Phi}_{\mathrm{f}}\right)^{-1}\boldsymbol{\Phi}_{\mathrm{f}}^{\mathrm{T}}\boldsymbol{y}_{\mathrm{f}} \tag{4.7}$$

which can be used to find $A_{\mathrm{f}}(z)$ for the next iteration. During the first iteration, the filtering polynomial $A_{\mathrm{f}}(z) = 1$. The iterations are continued until the estimated parameters converge to form the final values. It is important to check that the roots of $A_{\mathrm{f}}(z)$ are inside the unit circle after each iteration.

Publication VII introduces the required matrices $\boldsymbol{y}_{\mathrm{f}}$ and $\boldsymbol{\Phi}_{\mathrm{f}}$ for estimating the parameters of a two-mass system when the torque-control loop is assumed to be ideal. Moreover, the system can not be loaded during the identification process. On the other hand, Publication VI introduces the required matrices $\boldsymbol{y}_{\mathrm{f}}$ and $\boldsymbol{\Phi}_{\mathrm{f}}$ for the same case, but this time the torque-control loop dynamics [see (2.14)] can be included and the system can be loaded during the identification.

It is worth noting that several other iterative and recursive methods have been proposed to estimate the OE model without causing bias to

the parameter estimates. Textbook [111] provides a nice overview of these methods.

4.2.5 Continuous-Time Mechanical Parameters

Once the discrete-time two-mass system model has been identified, the obtained pulse-transfer function $B_{\mathrm{M,d}}(z)/A_{\mathrm{d}}(z)$ is first converted into a zero-pole, matching-equivalent, continuous-time transfer function:

$$\frac{y(s)}{u(s)} = \frac{b_1 s^2 + b_2 s + b_3}{s^3 + a_1 s^2 + a_2 s + a_3} \tag{4.8}$$

where $b_1 \dots b_3$ and $a_1 \dots a_3$ are the continuous-time transfer function coefficients. The relationship between these coefficients and the estimated discrete-time transfer function parameters $\boldsymbol{\theta}$ can be obtained either numerically or by using the analytical relations. The analytical relations are given in the Appendix of Publication VII. When comparing (2.5) and (4.8), the following system of equations is obtained:

$$b_1 = \frac{1}{J_{\mathrm{M}}} \tag{4.9a}$$

$$b_2 = \frac{c_{\mathrm{S}} + b_{\mathrm{L}}}{J_{\mathrm{M}} J_{\mathrm{L}}} \tag{4.9b}$$

$$b_3 = \frac{K_{\mathrm{S}}}{J_{\mathrm{M}} J_{\mathrm{L}}} \tag{4.9c}$$

$$a_1 = \frac{(J_{\mathrm{M}} + J_{\mathrm{L}}) c_{\mathrm{S}} + J_{\mathrm{L}} b_{\mathrm{M}} + J_{\mathrm{M}} b_{\mathrm{L}}}{J_{\mathrm{M}} J_{\mathrm{L}}} \tag{4.9d}$$

$$a_2 = \frac{(J_{\mathrm{M}} + J_{\mathrm{L}}) K_{\mathrm{S}} + (b_{\mathrm{M}} + b_{\mathrm{L}}) c_{\mathrm{S}} + b_{\mathrm{M}} b_{\mathrm{L}}}{J_{\mathrm{M}} J_{\mathrm{L}}} \tag{4.9e}$$

$$a_3 = \frac{K_{\mathrm{S}} (b_{\mathrm{M}} + b_{\mathrm{L}})}{J_{\mathrm{M}} J_{\mathrm{L}}} \tag{4.9f}$$

From (4.9), the mechanical parameters J_{M}, J_{L}, b_{M}, b_{L}, K_{S}, and c_{S} can be solved.

Publication VII demonstrates that the parameters of a two-mass system can be estimated without difficulties both in the open loop and in the closed speed-control loop, provided that ideal torque-control loop dynamics are assumed, the speed controller is known, and the system is not loaded during the identification. As an example, the system-parameter estimates of a tooth-belt coupled two-mass system (see Section 5.1) are given in Table 4.2. The parameters were estimated using the indirect closed-loop method and the direct closed-loop method. In both the cases, a simple proportional-type feedback controller was applied and the parameters were estimated at 200 rpm constant speed. It can be seen that both the indirect method and the direct method provided parameter estimates close to the datasheet-based parameters.

Table 4.2. Datasheet values and estimated mechanical parameters of the tooth-belt coupled two-mass system.

Parameter	Datasheet	Direct	Indirect
J_{M} (kgm^2)	0.005	0.0069	0.0066
J_{L} (kgm^2)	0.038	0.045	0.039
K_{S} (Nm/rad)	1100	1414	1374
c_{S} (Nms/rad)	0.22	1.27	1.12
b_{M} (Nms/rad)	0	-1.5	-1.39
b_{L} (Nms/rad)	0	1.58	1.4

Table 4.3. Datasheet values and estimated mechanical parameters of the shaft coupled two-mass system.

Parameter	Datasheet	Estimated
J_{M} (kgm^2)	0.01	0.01
J_{L} (kgm^2)	0.01	0.011
K_{S} (Nm/rad)	24000	24500
c_{S} (Nms/rad)	1.10	0.67
b_{M} (Nms/rad)	0	-3.96
b_{L} (Nms/rad)	0	3.97

On the other hand, Publication VI demonstrates that the proposed indirect closed-loop identification method can also be applied to estimate the parameters of a two-mass system, even if the torque-control loop bandwidth is lower than the mechanical-resonance frequency and if the system is loaded during the identification. However, it should be kept in mind, that both the the speed controller and the bandwidth of the torque controller have to be known a priori. As an example, the system-parameter estimates of a shaft coupled two-mass system (see Section 5.2) are given in Table 4.3. The parameters were estimated during a speed-step response test. Furthermore, a load-torque step was applied into the system during the parameter estimation. It can be seen that again the estimated parameters correspond well with the datasheet-based parameters.

It can be seen that in all three cases, an estimate of the motor-side damping b_{M} is negative. On the other hand, the sum $b_{\mathrm{M}} + b_{\mathrm{L}}$ of the viscous damping estimates is positive. Furthermore, when substituting the obtained parameter values back to the open-loop transfer function (4.8), all the coefficients of the transfer function are positive, meaning that the poles and zeros are located on the left half of the s-plane.

4.3 Non-Linearities

If the identified system is highly nonlinear, the linear identification methods presented in this chapter can be augmented with methods for estimating the nonlinear elements, such as backlash or friction [114–116]. A limit-cycle based continuous-time method is proposed in [117] for calculating of the resonance frequency of a nonlinear two-mass system. If the load inertia and the coupling stiffness vary during the drive operation (see Publication I and [36]), the proposed identification methods could be used to estimate the parameters of the mechanical system at various operating points; then it will be possible to construct a look-up table of parameter values as a function of the operating point. Moreover, if the nonlinearity can be parametrized in the state variables (e.g., Coulomb friction), it may be introduced in the predictor vector ϕ in (4.5) [29].

4.4 Model Validation

Model validation is an essential part of the identification procedure. The control designer needs to know whether the selected model structure and the identification setup offer good enough information about the real system. A common validation tool is residual analysis. Residual analysis is based on the statistical properties of the residuals $\varepsilon(k) = y(k) - \hat{y}(k)$, which is illustrated in Fig. 4.2. The simulated system output is denoted as $\hat{y}(k) = G_\mathrm{d}(z)u(k)$, where $G_\mathrm{d}(z)$ represents the zero-pole equivalent discretization of the continous-time time transfer function (2.5), which is obtained using the estimated system parameters.

The autocorrelation

$$R_\varepsilon(\tau) = \frac{1}{N}\sum_{k=1}^{N}\varepsilon(k)\varepsilon(k-\tau) \tag{4.10}$$

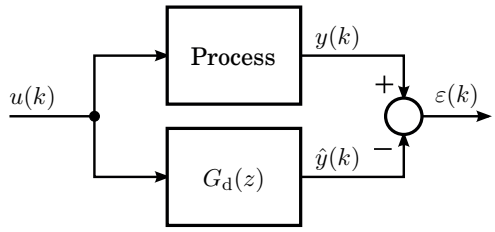

Figure 4.2. Validation using the residual analysis (see Publication VII). The transfer function $G_\mathrm{d}(z)$ represents the zero-pole equivalent discretization of the continous-time time transfer function (2.5).

of the residuals should ideally resemble that of white noise. Furthermore, the cross-correlation

$$R_{\varepsilon,u}(\tau) = \frac{1}{N}\sum_{k=1}^{N}\varepsilon(k)u(k-\tau) \tag{4.11}$$

between the input signal and the residuals should ideally be zero [111]. For the OE model, the emphasis in the residual analysis is on the cross-correlation since a noise model is not included in the OE structure [118]. If possible, the residual analysis should be performed using a different input-output dataset than the one used for the parameter estimation. Moreover, the identified model can be validated by comparing the time- and frequency-domain responses of the identified and measured (real) systems.

The parameter estimates obtained from (4.9) are analyzed by means of stochastical analysis. The cross-correlation between the input signal and the residuals is evaluated using (4.11). Figs. 4.3(a) and 4.4 show the results of the cross-correlation analysis for the parameter estimates given in Tables 4.2 and 4.3, respectively. A 97% confidence limit and a practical confidence limit are introduced in the figures [111]. The 97% confidence limit is calculated as $2.17/\sqrt{N}$, where N is the number of samples used in the estimation. Cross-correlation values remaining below the practical confidence limit will indicate that stochastically acceptable parameter estimates are obtained. It can be seen that the cross-correlations between the input and the residuals remain mostly below the practical confidence limit in all the cases.

Furhermore, the frequency responses, obtained using the datasheet parameter values and the estimated parameter values (given in Table 4.2), are compared in Fig. 4.3(b). It can be seen that the estimated frequency responses agree well with the datasheet-based frequency responses. It should be noted that the estimated amplitudes at the resonance frequencies are not directly comparable with the datasheet-based amplitudes, because $b_{\mathrm{M}} = b_{\mathrm{L}} = 0$ are assumed in the case of datasheet values. Furthermore, the datasheet values of c_{S} are only rough approximations, obtained using (2.13).

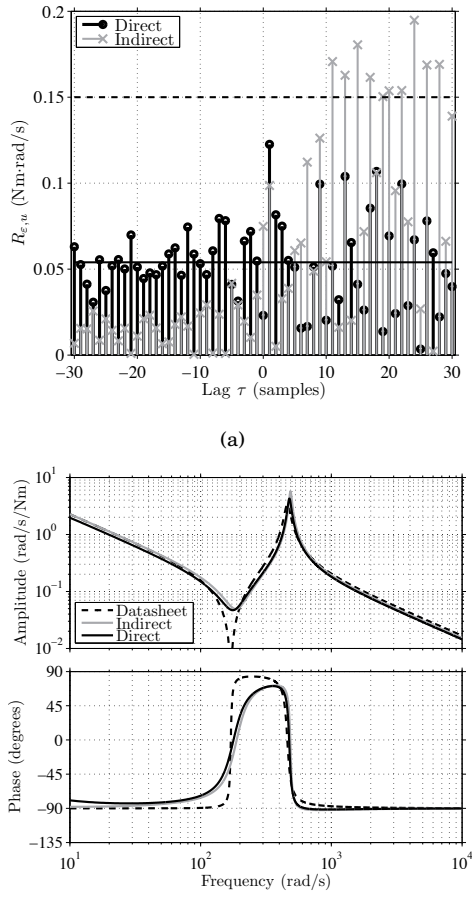

Figure 4.3. Validation of the parameters given in Table 4.2: (a) cross correlation between the input signal and the residuals; and (b) frequency response comparisons.

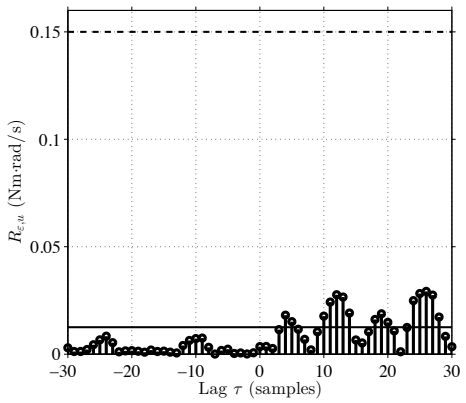

Figure 4.4. Validation of parameters given in Table 4.3: cross correlation between the input signal and the residuals.

5. Experimental Setups

Two experimental setups were used to experimentally test the methods described in Chapters 3 and 4. The basic configuration of both the setups is shown in Fig. 5.1. In both setups, a frequency-converter supplied, permanent-magnet synchronous motor (PMSM), controlled with a dSPACE board, was used as a driving motor. The driving motor was connected to a loading servo PMSM using a mechanical coupling. Section 5.1 introduces a setup where tooth belts are used as mechanical coupling between the motors, while Section 5.2 introduces a setup where a shaft is used for mechanical coupling between the two PMSMs.

5.1 Tooth-Belt Coupled Motors

The tooth-belt coupled PMSMs, shown in Fig. 5.2, were used in Publication IV, Publication VII, and Publication VIII. Different belts can be used to vary the coupling stiffness. An additional inertia disk can be added to the shaft of the load motor. Detailed information about the setup is provided in Table 5.1.

The mechanical-parameter configurations used in the design examples in Sections 3.4 and 3.5 are given in Tables 5.2 and 5.3, respectively.

5.2 Shaft-Coupled Motors

The shaft-coupled PMSMs were used in Publication II, Publication III, Publication V and Publication VI. Detailed information about the setup is provided in Table 5.4

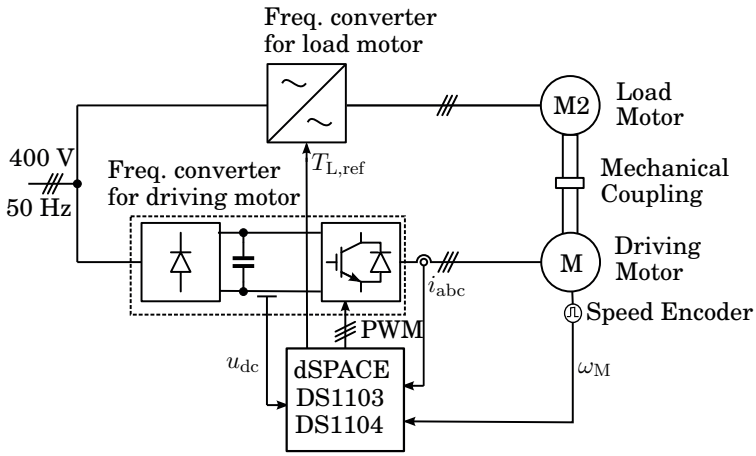

Figure 5.1. Experimental setup.

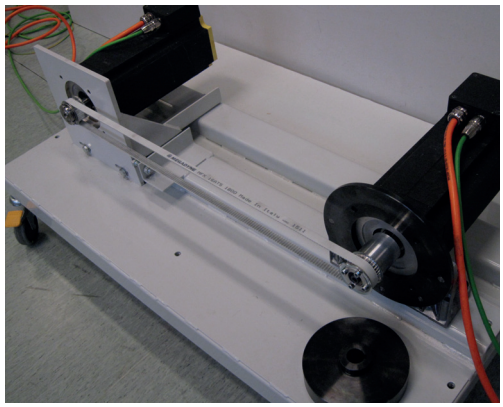

Figure 5.2. Tooth-belt coupled motors.

5.3 Mechanical-Load Emulation

Sometimes it is not possible (or it is not economically feasible) to arrange a testing environment for the testing the control or identification algorithms for complex mechanical loads. In such cases, a dynamic emulation (or hardware-in-the-loop simulation) may offer a versatile solution [119]. The complex mechanical systems can be mimicked using a dynamic emulation if the driving motor is rigidly connected to a controlled load machine. Then, the torque of the load machine can be used to mimic the dynamic behavior of the complex mechanics.

Publication II proposes a straightforward and practical method for dynamic emulation of multi-mass mechanical systems. The test bench described in Table 5.4 was applied, and the torque reference $T_{\mathrm{L,ref}}$ of the servo motor, cf. Fig. 5.1, was controlled based on the dynamic model to

Table 5.1. Technical data for the tooth-belt coupled setup (the output currents of the frequency converters are for an 8 kHz switching frequency)

Driving PMSM	**Baldor BSM 100N-4250-AF**
Rating plate	380 V, 50 Hz, 2400 rpm
Motor moment of inertia	0.005 kgm^2
Incremental encoder line count	2500 ppr
Load PMSM	**Baldor BSM 100N-4250-AD**
Rating plate	380 V, 50 Hz, 2400 rpm
Motor moment of inertia	0.005 kgm^2
Additional-inertia disc	0.034 kgm^2
Absolute encoder (EnDat) line count	2048 ppr
Freq. converters	**ABB ACSM1-04AM-031A-4**
Supply voltage	380...480 V
Supply current	23.3...7.1 A
Supply frequency	48...63 Hz
Output voltage	0...100% of supply voltage
Rated output current	31 A
Maximum output current	43 A
Output frequency	0...500 Hz
Toothed belts	**Megadyne Megaflex**
Tooth width	5 mm
Belt length	1800 mm
Distance between motor shafts	813.6 mm
Torsional stiffness (16 mm belt width)	650 Nm/rad
Torsional stiffness (20 mm belt width)	850 Nm/rad
Torsional stiffness (25 mm belt width)	1100 Nm/rad

be emulated. The angular speed and position need to be measured. Additionally, the electromagnetic torque of the driving motor is needed. When the electromagnetic torque is known, there is no need for inverse transfer functions or acceleration signals.

Table 5.2. Mechanical parameters used in Section 3.4

Parameter	J_{M} [kgm^2]	J_{L} [kgm^2]	K_{S} [Nm/rad]	c_{S} [Nms/rad]
Value	0.005	0.005	1100	0.11

Table 5.3. Mechanical parameters used in Section 3.5

Parameter	J_{M} [kgm^2]	J_{L} [kgm^2]	K_{S} [Nm/rad]	c_{S} [Nms/rad]
Value	0.005	0.039	650	0.065

Table 5.4. Technical data for the shaft-coupled setup

Driving PMSM	**ABB M2BJ 100L 6 B3**
Rating plate	370 V, 4.3 A, 75 Hz 1500 rpm
	1500 rpm, 2.2 kW, cos ϕ = 0.9
Motor moment of inertia	0.008 kgm^2
Incremental encoder line count	2048 ppr
Freq. conv. for driving PMSM	**Danfoss VLT5004 P T5 B20 EB R3**
Supply voltage	380. . .500 V (50/60 Hz)
Output voltage	0. . .100% of supply voltage
Maximum const. output current	5.6 A
Output frequency	0. . .1000 Hz
Load PMSM	**ABB 8C5 230 00YA02SL3MB**
Rating plate	315 V, 2400 rpm
Constant stall torque	21.5 Nm (14.1 A)
Peak stall torque	75.3 Nm (54.6 A)
Motor moment of inertia	0.008 kgm^2
Freq. conv. for load PMSM	**ABB Bivector 353 “25"**
Rated supply voltage	400 V (50/60 Hz)
Rated output voltage	400 V
Rated cont. output current	25 A
Mechanical coupling	**HBM BSD-MODULFLEX for K-T10F**
Torsional stiffness	24 kNm/rad
Moment of inertia	0.0029 kgm2

6. Summaries of Publications

6.1 Abstracts

The abstracts of the publications are reprinted in this section.

Publication I

Production rate plays an important role in industrial applications, which means higher demands for accelerations and speeds of the systems. The requirements for accuracy and repeatability are also increasing. A solution for these demands is a high-speed tooth belt linear drive; however, the drawbacks of system of this kind are non-linear friction and flexibility of the belt, which make the precision control of the system difficult. In this paper, the frictions and flexibility of the high-speed tooth belt linear drive are analyzed.

Publication II

This paper presents a straightforward method for dynamic emulation of multi-mass systems. The test bench consists of a driving motor coupled rigidly to a load servo motor, and the torque reference of the servo motor is controlled based on the dynamic model to be emulated. No additional measurements are needed, but the mechanical parameters of the test bench and the torque estimate of the driving motor have to be known. The use of the torque estimate makes it possible to avoid using any differentiations or controller compensation terms in the emulator. The experimental results show that the emulator can model the dynamics of the multi-mass mechanical load with a good accuracy. In addition, the robustness against the mechanical parameter inaccuracies is good.

Publication III

This paper presents a method for parameter estimation of a two-mass mechanical loads. A discrete time polynomial model with an output er-

ror (OE) structure is used in parameter estimation. Open- and closed-loop cases are analyzed. Different input and output signals can be selected in closed-loop identification. Four different identification setups are analyzed and the identifiabilities are compared. It is discovered that all the four identification setups can be used to obtain reasonable parameter estimates.

Publication IV

This paper deals with model-based two-degrees-of-freedom (2DOF) speed control of two-mass systems. An analytic gain selection of a proportinal integral (PI) type feedback controller is proposed. The gains are given as functions of system parameters and desired dominant closed-loop poles. An analytic design of a prefilter is given to complete the 2DOF structure, using the pole-zero distribution of the feedback loop. The prefilter design covers step, ramp, and parabolic reference tracking. The proposed 2DOF controller is evaluated by means of simulations and experiments. The experimental setup consists of two 4-kW servo motors coupled together with a toothed belt. It was found that the proposed controller gives good reference tracking for step and dynamic commands as well as robust and fast load-torque rejection.

Publication V

A classical-control approach to the design and analysis of proportional–integral (PI) speed controllers for electrical drives is presented. After vindicating the fact that traditional one-degree-of-freedom PI control generally gives unsatisfactory performance, a well-performing two-degrees-of-freedom PI controller is designed, with analytic parameter selection. The robustness of the obtained closed-loop system is analyzed, and is found to be satisfactory. All the proposed control designs are validated by means of experiments.

Publication VI

This paper presents a method to identify the parameters of a two-mass mechanical system, when the system is operating in closed-loop speed control. When the speed and the torque controllers are known, the proposed method can be applied for the parameter estimation of a system, which has a higher mechanical resonance frequency than the torque-control loop bandwidth. Moreover, if the loading torque is known a priori, the method may be used for systems that are loaded during the identification.

Publication VII

This paper deals with methods for parameter estimation of two-mass me-

chanical systems in electric drives. Estimates of mechanical parameters are needed in the start-up of a drive for automatic tuning of model-based speed and position controllers. A discrete-time output error (OE) model is applied to parameter estimation. The resulting pulse-transfer function is transformed into a continuous-time transfer function, and parameters of the two-mass system model are analytically solved from the coefficients of this transfer function. An open-loop identification setup and two closed-speed-loop identification setups (direct and indirect) are designed and experimentally compared. The experiments are carried out at nonzero speed, making the closed-loop identification setup easier to apply. It was found out that all the identification setups are applicable for the parameter estimation of two-mass mechanical systems.

Publication VIII

This paper proposes a model-based two-degrees-of-freedom (2DOF) state-space speed controller design for a two-mass mechanical system. Analytical tuning rules for a feedback gain, a reduced-order state observer, a full-order state observer, and a prefilter are derived. The proposed design rules enable automatic tuning of the controller if the mechanical parameters are known. The prefilter is designed for step, ramp, and parabolic command tracking. It is shown by Nyquist diagrams and noise-transfer functions that the full-order observer based controller is a preferable choice if the feedback loop is delayed and noisy. Time-domain simulations and experimental results verified the Nyquist-diagram analysis and showed that the proposed controller gives good reference tracking for step and dynamic commands as well as robust and fast load-torque rejection.

6.2 Scientific Contribution

The main scientific contributions of this dissertation can be summarized as follows.

Publication I

The paper introduces the friction behavior and nonlinear resonance frequencies of a tooth-belt-driven motion control system.

Publication II

The paper proposes and validates a robust and measurement-noise insensitive method for the dynamic emulation of complex mechanical loads in electric drives. The algorithm is based on the motor-torque estimate instead of acceleration or inverse models.

Publication III

The paper proposes a discrete-time indirect closed-loop method for identifying a two-mass mechanical system. The method is tested by applying the emulation method proposed in Publication II.

Publication IV

The main contribution of this paper is the analytical tuning of a PI-based 2DOF controller for two-mass mechanical systems. The analytical tuning is based on the placement of the dominant feedback-loop poles and on improving the command tracking by introducing a prefilter.

Publication V

This paper demonstrates (analytically and by using experiments) that a properly designed classical 2DOF controller is a well-suited and robust option for the speed control of single-mass systems.

Publication VI

The main contribution of this paper is that it tackles the difficulties of closed-loop identification by introducing a modified indirect method that can be used to find the same mechanical parameter estimates as in Publication VII. This can be done even if the speed controller is more complex, if the mechanical resonance frequency is higher than the torque-control loop bandwidth, and if the system is loaded during the identification process.

Publication VII

The main contribution of this paper is to improve the methods proposed in Publication III by introducing an adaptive OE method and analytical relations between the discrete-time transfer function coefficients and the continuous-time mechanical parameters. Furthermore, the indirect identification method is experimentally compared with the open-loop identification method, the direct identification method, and the frequency-response based method.

Publication VIII

The main contribution is the analytical tuning of an observer-based 2DOF state-space controller for a two-mass mechanical systems. Particularly, the closed-loop pole locations are proposed for delayed and noisy feedback-loop conditions.

7. Conclusions

Because ac electric drives have been increasingly selected as a torque or force actuators in motion control devices, the development of different speed-control methods has been a point of interest for nearly the past forty years. Both the classical control methods (i.e., PI-based controllers and state-space controllers) as well as quite complex nonlinear control methods can be found in the literature. Unfortunately, the classical controllers are often tuned based on some heuristic approach or by using, for example, the step-response based Ziegler-Nichols tuning rules. Moreover, when justifying the selection of the complex nonlinear controllers, the nonlinear controller is incorrectly compared only with poorly tuned classical controllers.

One of the most important findings of this dissertation is that the classical control methods are still very well suited for the speed and position control of electric drives. The dissertation demonstrated that it is possible to obtain a well-performing and robust 2DOF speed controller provided that the controller tuning is done in an appropriate manner. Instead of trial-and-error tuning or applying some step-response based iterative method, it was shown that model-based pole placement is a powerful tool.

It is evident that the model-based control design requires information about the parameters of the system model. The dissertation demonstrated that if the designers rely solely on manufacturers' datasheets, it will be difficult to find reasonable values for the mechanical parameters. Instead, a well-established parameter-identification routine should be applied. It was found out that the polynomial-model based discrete-time OE method is a better alternative than frequency-response based methods. This is mainly because of the absence of the time domain to the frequency domain conversion, which adds an additional computational burden and numerical inaccuracies to the identification method. It was shown that

the proposed OE method can be applied both in the open-loop and in the closed-loop configurations.

The future research work dealing with the topic of speed control might include the implementation and testing of a gain-scheduled 2DOF speed controller. This would also require developing and implementing an on-line parameter-identification routine. To improve system robustness, the 2DOF speed control design could be carried out by applying the Nyquist diagrams and by analytically showing that the system will remain stable within certain parameter range. Moreover, the 2DOF controller could be augmented with an anti-windup algorithm, which can reduce the residual vibrations appearing when the output of the system is saturated.

On the other hand, future research work on the topic of identification could include parameter estimation for the three-mass systems and an automatic decisions about a suitable system model for different mechanical loads. Furthermore, the identification routines could be modified to exclude the viscous-damping coefficients from the identification process. An alternative approach would be to estimate the sum of the viscous-damping coefficients. This would remove the problem of negative viscous-damping coefficient estimates.

Bibliography

[1] K. Ohnishi, M. Shibata, and T. Murakami, "Motion control for advanced mechatronics," *IEEE/ASME Trans. Mechatronics*, vol. 1, no. 1, pp. 56–67, Mar. 1996.

[2] F. Blaschke, "The principle of field orientation as applied to the new transvector closed-loop control system for rotating field machine," *Siemens Rev.*, vol. 34, no. 5, pp. 217–220, 1972.

[3] I. Takahashi and T. Noguchi, "A new quick-response and high-efficiency control strategy of an induction motor," *IEEE Trans. Ind. Appl.*, vol. IA-22, no. 5, pp. 820–827, Sept. 1986.

[4] M. Depenbrock, "Direct self-control (DSC) of inverter-fed induction machine," *IEEE Trans. Power Electron.*, vol. 3, no. 4, pp. 420–429, Oct. 1988.

[5] K. Ohishi and R. Furusawa, "Actuators for motion control: Fine actuator force control for electric injection molding machines," *IEEE Ind. Electron. Mag.*, vol. 6, no. 1, pp. 4–13, Mar. 2012.

[6] C. Hu, B. Yao, and Q. Wang, "Coordinated adaptive robust contouring controller design for an industrial biaxial precision gantry," *IEEE/ASME Trans. Mechatronics*, vol. 15, no. 5, pp. 728–735, Oct. 2010.

[7] M.-S. Tsai, C.-L. Yen, and H.-T. Yau, "Integration of an empirical mode decomposition algorithm with iterative learning control for high-precision machining," *IEEE/ASME Trans. Mechatronics*, vol. 18, no. 3, pp. 878–886, June 2013.

[8] M. Östring, S. Gunnarsson, and M. Norrlöf, "Closed-loop identification of an industrial robot containing flexibilities," *Control Engineering Practice*, Mar. 2003.

[9] J. Park, P.-H. Chang, H.-S. Park, and E. Lee, "Design of learning input shaping technique for residual vibration suppression in an industrial robot," *IEEE/ASME Trans. Mechatronics*, vol. 11, no. 1, pp. 55–65, Feb. 2006.

[10] P. K. Nandam and P. C. Sen, "Analog and digital speed control of DC drives using proportional-integral and integral-proportional control techniques," *IEEE Trans. Ind. Electron.*, vol. IE-34, no. 2, pp. 227–233, May 1987.

[11] L. J. Garces, "Parameter adaption for the speed-controlled static AC drive with a squirrel-cage induction motor," *IEEE Trans. Ind. Appl.*, vol. IA-16, no. 2, pp. 173–178, Mar. 1980.

[12] I. Takahashi and Y. Ohmori, "High-performance direct torque control of an induction motor," *IEEE Trans. Ind. Appl.*, vol. 25, no. 2, pp. 257–264, Mar./Apr. 1989.

[13] M. Tomizuka, "Zero phase error tracking algorithm for digital control," *Journal of Dyn. Syst., Meas., and Cont.*, vol. 109, no. 1, pp. 65–68, Mar. 1987.

[14] C.-M. Liaw, Y.-S. Kung, and C.-M. Wu, "Design and implementation of a high-performance field-oriented induction motor drive," *IEEE Trans. Ind. Electron.*, vol. 38, no. 4, pp. 275–282, Aug. 1991.

[15] M. Koyama, "A microprocessor-based motor speed regulator using fast-response state observer for reduction of torsional vibration," *Trans. IEE-J*, vol. 107-D, pp. 1010–1017, Sept. 1987.

[16] T. Ohmae, T. Matsuda, M. Kanno, K. Saito, and T. Sukegawa, "A microprocessor-based motor speed regulator using fast-response state observer for reduction of torsional vibration," *IEEE Trans. Ind. Appl.*, vol. IA-23, no. 5, pp. 863–871, Sept. 1987.

[17] R. Dhaouadi, K. Kubo, and M. Tobise, "Two-degree-of-freedom robust speed controller for high-performance rolling mill drives," *IEEE Trans. Ind. Appl.*, vol. 29, no. 5, pp. 919–923, Sep./Oct. 1993.

[18] Y. Hori, H. Iseki, and K. Sugiura, "Basic consideration of vibration suppression and disturbance rejection control of multi-inertia system using SFLAC (state feedback and load acceleration control)," *IEEE Trans. Ind. Appl.*, vol. 30, no. 4, pp. 889–896, Jul./Aug. 1994.

[19] J.-K. Ji and S.-K. Sul, "Kalman filter and LQ based speed controller for torsional vibrations suppression in a 2-mass motor drive system," *IEEE Trans. Ind. Electron.*, vol. 42, no. 6, pp. 564–571, Dec. 1995.

[20] B. Yao and C. Jiang, "Advanced motion control: From classical PID to nonlinear adaptive robust control," in *Proc. IEEE AMC'10*, Mar. 2010, pp. 815–829.

[21] K. Åström and T. Hägglund, "The future of PID control," *Cont. Eng. Pract.*, vol. 9, pp. 1163–1175, Nov. 2001.

[22] M. Iwasaki, K. Seki, and Y. Maeda, "High-precision motion control techniques: A promising approach to improving motion performance," *IEEE Ind. Electron. Mag.*, vol. 6, no. 1, pp. 32–40, Mar. 2012.

[23] S. N. Vukosavic and M. R. Stojic, "Suppression of torsional oscillations in a high-performance speed servo drive," *IEEE Trans. Ind. Electron.*, vol. 45, no. 1, pp. 108–117, Feb. 1998.

[24] T. Miyazaki and K. Ohishi, "Robust speed control system considering vibration suppression caused by angular transmission error of planetary gear," *IEEE/ASME Trans. Mechatronics*, vol. 7, no. 2, pp. 235–244, June 2002.

[25] H. Zoubek, S. Villwock, and M. Pacas, "Frequency response analysis for rolling-bearing damage diagnosis," *IEEE Trans. Ind. Electron.*, vol. 55, no. 12, pp. 4270–4276, Sep. 2008.

[26] L. Ljung, *System Identification: Theory for the User*, 2nd ed. Troy, NY: Prentice-Hall, 1999.

[27] S. Villwock and M. Pacas, "Application of the Welch-method for the identification of two- and three-mass-systems," *IEEE Trans. Ind. Electron.*, vol. 55, no. 1, pp. 457–466, Jan. 2008.

[28] S. Beineke, F. Schütte, H. Wertz, and H. Grotstollen, "Comparison of parameter identification schemes for self-commissioning drive control of nonlinear two-mass systems," in *IEEE IAS Conf.*, vol. 1, New Orleans, LA, Oct. 1997, pp. 493–500.

[29] H. Wertz, S. Beineke, N. Frohleke, S. Bolognani, K. Unterkofler, M. Zigliotto, and M. Zordan, "Computer aided commissioning of speed and position control for electrical drives with identification of mechanical load," in *IEEE IAS Conf.*, vol. 4, Phoenix, AZ, Oct. 1999, pp. 2372–2379.

[30] I. D. Landau and A. Karimi, "An output error recursive algorithm for unbiased identification in closed loop," *Automatica*, vol. 33, no. 5, pp. 933–938, May 1997.

[31] I. Müller and P. Mutschler, "Two reliable methods for estimating the mechanical parameters of a rotating three-inertia system," in *EPE-PEMC 2002 Conf.*, Cavtat and Dubrovnik, Croatia, Sep. 2002, CD-ROM.

[32] J.-K. Kang and S.-K. Sul, "Vertical-vibration control of elevator using estimated car acceleration feedback compensation," *IEEE Trans. Ind. Electron.*, vol. 47, no. 1, pp. 91–99, Feb. 2000.

[33] K. K. Varanasi and S. A. Nayfeh, "The dynamics of lead-screw drives: Low-order modeling and experiments," *ASME J. Dyn. Syst., Meas., Control*, vol. 126, pp. 388–396, June 2009.

[34] S. G. Kelly, *Mechanical Vibrations: Theory and Applications*. Stamford, CT: Cengage Learning, 2011.

[35] S. Saarakkala, M. Haapala, M. Jokinen, M. Niemelä, R. Pöllänen, and J. Pyrhönen, "Performance, limitations, and control of a high-speed tooth belt drive in a motion control application," in *Proc. IEEE EUROCON '09*, May 2009, pp. 835–842.

[36] M. Jokinen, *Centralized motion control of a linear tooth belt drive: analysis of the performance and limitations*, D.Sc. Dissertation, Lappeenranta University of Technology, Lappeenranta, Finland, 2010.

[37] A. Frei, A. Grgic, W. Heil, and A. Luzi, "Design of pump shaft trains having variable-speed electric motors," in *International Pump Symposium*, Houston, TX, May 1986, pp. 33–44.

[38] L. Harnefors and H.-P. Nee, "Model-based current control of AC machines using the internal model control method," *IEEE Trans. Ind. Appl.*, vol. 34, no. 1, pp. 133–141, Jan./Feb. 1998.

[39] W. Leonhard, *Control of Electrical Drives*, 3rd ed. Berlin, Germany: Springer, 2001.

[40] J. Vaughan, D. Kim, and W. Singhose, "Control of tower cranes with double-pendulum payload dynamics," *IEEE Trans. Cont. Syst, Tech.*, vol. 18, no. 6, pp. 1345–1358, Nov. 2010.

[41] N. Mutoh, "Driving and braking torque distribution methods for front- and rear-wheel-independent drive-type electric vehicles on roads with low friction coefficient," *IEEE Trans. Ind. Electron.*, vol. 59, no. 10, pp. 3919–3933, Oct. 2012.

[42] B. Armstrong-Hélouvry, P. Dupont, and C. Canudas de Wit, "A survey of models, analysis tools and compensation methods for the control of machines with friction," *Automatica*, vol. 30, no. 7, p. 1083–1138, July 1994.

[43] M. Nordin and P.-O. Gutman, "Controlling mechanical systems with backlash—a survey," *Automatica*, vol. 38, no. 10, pp. 1633–1649, Oct. 2002.

[44] R. Muszynski and J. Deskur, "Damping of torsional vibrations in high-dynamic industrial drives," *IEEE Trans. Ind. Electron.*, vol. 57, no. 2, pp. 544–552, Feb. 2010.

[45] R. Petrella, M. Tursini, L. Peretti, and M. Zigliotto, "Speed measurement algorithms for low-resolution incremental encoder equipped drives: a comparative analysis," in *Proc. IEEE ACEMP '07*, Sept. 2007, pp. 780–787.

[46] A. Kosonen, M. Jokinen, J. Ahola, M. Niemelä, and J. Toukonen, "Ethernet-based broadband power line communication between motor and inverter," *IET Proc.—Electr. Power Appl.*, vol. 2, no. 5, pp. 316–324, Sep. 2008.

[47] K. K. Tan and A. S. Putra, *Drives and Control for Industrial Automation*. London, United Kingdom: Springer, 2011.

[48] P. K. Nandam and P. C. Sen, "Analog and digital speed control of dc drives using proportional-integral and integral-proportional control techniques," *IEEE Trans. Ind. Electron.*, vol. IE-34, no. 2, pp. 227–234, May 1987.

[49] J. Y. Hung, R. M. Nelms, and P. B. Stevenson, "An output feedback sliding mode speed regulator for dc drives," *IEEE Trans. Ind. Appl.*, vol. 30, no. 3, pp. 691–698, May/Jun. 1994.

[50] C.-M. Liaw and C.-M. Wu, "Design and implementation of a high-performance field-oriented induction motor drive," *IEEE Trans. Ind. Electron.*, vol. 38, no. 4, pp. 275–282, Aug. 1991.

[51] M. S. Huang and C. M. Liaw, "Speed control for field-weakening induction motor drive," *IEE Proc.—Electr. Power Appl.*, vol. 152, no. 3, pp. 565–576, May 2005.

[52] M. Jemli, H. Ben Azza, M. Boussak, and M. Gossa, "Sensorless indirect stator field orientation speed control for single-phase induction motor drive," *IEEE Trans. Power Electron.*, vol. 24, no. 6, pp. 1618–1627, Jun. 2009.

[53] A. Takano, "Quick-response torque-controlled induction motor drives under phase-locked loop speed control with disturbance compensation," *IEEE Trans. Ind. Electron.*, vol. 43, no. 6, pp. 640–646, Dec. 2009.

[54] G. Feng, Y.-F. Liu, and L. Huang, "A new robust algorithm to improve the dynamic performance on the speed control of induction motor drive," *IEEE Trans. Power Electron.*, vol. 19, no. 6, pp. 1614–1627, Nov. 2004.

[55] L. Zhen and L. Xu, "Fuzzy learning enhanced speed control of an indirect field-oriented induction machine drive," *IEEE Trans. Contr. Syst. Technol.*, vol. 8, no. 2, pp. 270–278, Mar. 2000.

[56] M. Masiala, B. Vafakhah, J. Salmon, and A. M. Knight, "Fuzzy self-tuning speed control of an indirect field-oriented control induction motor drive," *IEEE Trans. Ind. Appl.*, vol. 44, no. 6, pp. 1732–1740, Nov./Dec. 2008.

[57] Y. S. Kung, C. M. Liaw, and M. S. Ouyang, "Adaptive speed control for induction motor drives using neural networks," *IEEE Trans. Ind. Electron.*, vol. 42, no. 1, pp. 25–32, Feb. 1995.

[58] T.-C. Chen and T.-T. Sheu, "Model reference neural network controller for induction motor speed control," *IEEE Trans. Energy Convers.*, vol. 17, no. 2, pp. 157–163, Jun. 2002.

[59] K.-K. Shyu and H.-J. Shieh, "A new switching surface sliding-mode speed control for induction motor drive systems," *IEEE Trans. Power Electron.*, vol. 11, no. 4, pp. 660–667, Jul. 1996.

[60] C.-M. Liaw, Y.-M. Lin, and K.-H. Chao, "A VSS speed controller with model reference response for induction motor drives," *IEEE Trans. Ind. Electron.*, vol. 48, no. 6, pp. 1136–1147, Dec. 2001.

[61] M. Rashed, K. B. Goh, M. W. Dunnigan, P. F. A. MacConnell, A. F. Stronach, and B. W. Williams, "Sensorless second-order sliding-mode speed control of a voltage-fed induction-motor drive using nonlinear state feedback," *IEE Proc.—Electr. Power Appl.*, vol. 152, no. 5, pp. 1127–1136, Sep. 2005.

[62] K.-T. Chang, T.-S. Low, and T.-H. Lee, "An optimal speed controller for permanent-magnet synchronous motor drives," *IEEE Trans. Ind. Electron.*, vol. 41, no. 5, pp. 503–510, Oct. 1994.

[63] C. De Angelo, G. Bossio, G. Solsona, G. O. García, and M. Inéz Valla, "Mechanical sensorless speed control of permanent-magnet ac motors driving an unknown load," *IEEE Trans. Ind. Electron.*, vol. 53, no. 2, pp. 406–414, Apr. 2006.

[64] Y. A.-R. Mohamed, "Adaptive self-tuning speed control for permanent-magnet synchronous motor drive with dead time," *IEEE Trans. Energy Convers.*, vol. 21, no. 4, pp. 855–862, Dec. 2006.

[65] C. B. Butt, M. A. Hoque, and M. A. Rahman, "Simplified fuzzy-logic-based MTPA speed control of IPMSM drive," *IEEE Trans. Ind. Appl.*, vol. 40, no. 6, pp. 1529–1535, Nov./Dec. 2004.

[66] M. N. Uddin and M. M. I. Chy, "Online parameter-estimation-based speed control of PM AC motor drive in flux-weakening region," *IEEE Trans. Ind. Appl.*, vol. 44, no. 5, pp. 1486–1494, Dec. 2008.

[67] Y.-S. Kung and M.-H. Tsai, "FPGA-based speed control IC for PMSM drive with adaptive fuzzy control," *IEEE Trans. Power Electron.*, vol. 22, no. 6, pp. 2476–2486, Nov. 2007.

[68] M. A. Rahman and A. A. Hoque, "On-line self-tuning ANN-based speed control of a PM DC motor," *IEEE Trans. Mechatron.*, vol. 2, no. 3, pp. 169–178, Sep. 1997.

[69] I.-C. Baik, K.-H. Kim, and M.-J. Youn, "Robust nonlinear speed control of PM synchronous motor using adaptive and sliding mode control techniques," *IEE Proc.—Electr. Power Appl.*, vol. 145, no. 4, pp. 369–376, Nov. 1998.

[70] K. I. Hwu and C. M. Liaw, "Robust quantitative speed control of a switched reluctance motor drive," *IEE Proc.—Electr. Power Appl.*, vol. 148, no. 4, pp. 345–353, Jul. 2001.

[71] T.-S. Chuang and C. Pollock, "Robust speed control of a switched reluctance vector drive using variable structure approach," *IEEE Trans. Ind. Electron.*, vol. 44, no. 6, pp. 800–808, Dec. 1997.

[72] R. Dhaouadi, K. Kubo, and M. Tobise, "Two-degree-of-freedom robust speed controller for high-performance rolling mill drives," *IEEE Trans. Ind. Appl.*, vol. 29, no. 5, pp. 919–926, Sep./Oct. 1993.

[73] G. F. Franklin, J. D. Powell, and A. Emami-Naeini, *Feedback Control of Dynamic Systems*, 4th ed. Upper Saddle River, NJ: Prentice-Hall, 2002.

[74] C.-M. Liaw, "Design of a two-degrees-of-freedom controller for motor drives," *IEEE Trans. Autom. Contr.*, vol. 37, no. 8, pp. 1215–1220, Aug. 1992.

[75] C.-M. Liaw and S.-Y. Cheng, "Fuzzy two-degrees-of-freedom speed controller for motor drives," *IEEE Trans. Ind. Electron.*, vol. 42, no. 2, pp. 209–216, Apr. 1995.

[76] S. K. Chung, J. H. Lee, J. S. Ko, and M. J. Youn, "Robust speed control of brushless direct-drive motor using integral variable structure control," *IEE Proc.—Electr. Power Appl.*, vol. 142, no. 6, pp. 361–370, Nov. 1995.

[77] Z. Ibrahim and E. Levi, "A comparative analysis of fuzzy logic and PI speed control in high-performance ac drives using experimental approach," *IEEE Trans. Ind. Appl.*, vol. 38, no. 5, pp. 1210–1218, Sep./Oct. 2002.

[78] G. Ellis, *Control System Design Guide: A Practical Guide*. San Diego, CA: Elsevier, 2004.

[79] R. D. Lorenz and K. W. Van Patten, "High-resolution velocity estimation for all-digital, AC servo drives," *IEEE Trans. Ind. Appl.*, vol. 27, no. 4, pp. 701–705, Jul./Aug. 1991.

[80] G. Ellis and R. Lorenz, "Resonant load control methods for industrial servo drives," in *Conf. Rec. IEEE-IAS Annu. Meeting*, vol. 3, Rome, Italy, Oct. 2000, pp. 1438–1445.

[81] S. Thomsen, N. Hoffmann, and F. W. Fuchs, "PI control, PI-based state space control, and model-based predictive control for drive systems with elastically coupled loads — a comparative study," *IEEE Trans. Ind. Electron.*, vol. 58, no. 8, pp. 3647–3657, Aug. 2011.

[82] G. Zhang and J. Furusho, "Speed control of two-inertia system by PI/PID control," *IEEE Trans. Ind. Electron.*, vol. 47, no. 3, pp. 603–609, Jun. 2000.

[83] K. Szabat and T. Orlowska-Kowalska, "Vibration suppression in a two-mass drive system using PI speed controller and additional feedbacks — comparative study," *IEEE Trans. Ind. Electron.*, vol. 54, no. 2, pp. 1193–1206, Apr. 2007.

[84] W. Li and Y. Hori, "Vibration suppression using single neuron-based PI fuzzy controller and fractional-order disturbance observer," *IEEE Trans. Ind. Electron.*, vol. 54, no. 1, pp. 117–126, Feb. 2007.

[85] T. Atsumi, A. Okuyama, and M. Kobayashi, "Track-following control using resonant filter in hard disk drives," *IEEE/ASME Trans. Mechatronics*, vol. 12, no. 4, pp. 472–479, Aug. 2007.

[86] W. C. Messner, "Classical control revisited: Variations on a theme," in *Proc. IEEE AMC'08*, vol. 1, Trento, Italy, Mar. 2008, pp. 15–20.

[87] A. Hace, K. Jezernik, and A. Sabanovic, "SMC with disturbance observer for a linear belt drive," *IEEE Trans. Ind. Electron.*, vol. 54, no. 6, pp. 3402–3412, Dec. 2007.

[88] D. A. Bristow, M. Tharayil, and A. G. Alleyne, "A survey of iterative learning control," *IEEE Cont. Sys. Mag.*, vol. 26, no. 3, pp. 96–114, June 2006.

[89] K. Peter, I. Scholing, and B. Orlik, "Robust output-feedback H_∞ control with a nonlinear observer for a two-mass system," *IEEE Trans. Ind. Electron.*, vol. 39, no. 3, pp. 637–644, May/June 2003.

[90] E. J. Fuentes, C. A. Silva, and J. I. Yuz, "Predictive speed control of a two-mass system driven by a permanent magnet synchronous motor," *IEEE Trans. Ind. Electron.*, vol. 59, no. 7, pp. 2840–2848, July 2012.

[91] H.-B. Beck and D. Turschner, "Commissioning of a state-controlled high-powered electrical drive using evolutionary algorithms," *IEEE/ASME Trans. Mechatronics*, vol. 6, no. 2, pp. 149–154, June 2001.

[92] K. Szabat and T. Orlowska-Kowalska, "Performace improvement of industrial drives with mechanical elasticity using nonlinear adaptive Kalman filter," *IEEE Trans. Ind. Electron.*, vol. 54, no. 2, pp. 1193–1206, Apr. 2007.

[93] M. Cychowski, K. Szabat, and T. Orlowska-Kowalska, "Constrained model predictive control of the drive system with mechanical elasticity," *IEEE Trans. Ind. Electron.*, vol. 56, no. 6, pp. 1963–1973, June 2009.

[94] Y. Hori, H. Sawada, and C. Yeonghan, "Slow resonance ratio control for vibration suppression and disturbance rejection in torsional system," *IEEE Trans. Ind. Electron.*, vol. 46, no. 1, pp. 162–168, Feb. 1999.

[95] K. Saiki, A. Hara, K. Sakata, and H. Fujimoto, "A study on high-speed and high-precision tracking control of large-scale stage using perfect tracking control method based on multirate feedforward control," *IEEE Trans. Ind. Electron.*, vol. 57, no. 4, pp. 1393–1400, Apr. 2010.

[96] T. Atsumi, "Feedforward control using sampled-data polynomial for track seeking in hard disk drives," *IEEE Trans. Ind. Electron.*, vol. 56, no. 5, pp. 1338–1346, May 2009.

[97] G. F. Franklin, J. D. Powell, and M. L. Workman, *Digital Control of Dynamic Systems*, 3rd ed. Menlo Park, CA: Addison-Wesley, 1997.

[98] P. H. Meckl and R. Kinceler, "Robust motion control of flexible systems using feedforward forcing functions," *IEEE Trans. Contr. Sys. Tech.*, vol. 2, no. 3, pp. 245–254, 1994.

[99] M. Hirata, T. Hasegawa, and K. Nonami, "Seek control of hard disk drives based on final-state control taking account of the frequency components and the magnitude of control input," in *Proc. IEEE AMC'02*, vol. 1, Maribor, Slovenia, Mar. 2002, pp. 40–45.

[100] C.-W. Ha, K.-H. Rew, and K.-S. Kim, "Robust zero placement for motion control of lightly damped systems," *IEEE Trans. Ind. Electron.*, vol. 60, no. 9, pp. 3857–3864, 2013.

[101] S. Macfarlane and E. A. Croft, "Jerk-bounded manipulator trajectory planning: design for real-time applications," *IEEE Trans. Robot. Autom.*, vol. 19, no. 1, pp. 42–52, Feb. 2003.

[102] B.-H. Chang and Y. Hori, "Trajectory design considering derivative of jerk for head-positioning of disk drive system with mechanical vibration," *IEEE/ASME Trans. Mechatronics*, vol. 11, no. 3, pp. 273–279, June 2006.

[103] H. Li, M. D. Le, Z. M. Gong, and W. Lin, "Motion profile design to reduce residual vibration of high-speed positioning stages," *IEEE/ASME Trans. Mechatronics*, vol. 14, no. 2, pp. 264–269, Apr. 2009.

[104] V. A. Sujan and S. Dubowsky, "An optimal information method for mobile manipulator dynamic parameter identification," *IEEE/ASME Trans. Mechatronics*, vol. 2, no. 2, pp. 215–225, June 2003.

[105] R. Garrido and A. Concha, "An algebraic recursive method for parameter identification of a servo model," *IEEE/ASME Trans. Mechatronics*, 2013, early access.

[106] Y. Yoshioka and T. Hanamoto, "Estimation of a multimass system using the LWTLS and a coefficient diagram for vibration-controller design," *IEEE Trans. Ind. Appl.*, vol. 44, no. 2, pp. 566–574, Mar./Apr. 2008.

[107] L. Peretti and M. Zigliotto, "Identification of mechanical load for electrical drives commissioning - labelling machine case study," in *Proc. IEEE EUROCON '09*, May 2009, pp. 797–803.

[108] Z. Wang, Q. Zou, L. Faidley, and G.-Y. Kim, "Dynamics compensation and rapid resonance identification in ultrasonic-vibration-assisted microforming system using magnetostrictive actuator," *IEEE/ASME Trans. Mechatronics*, vol. 16, no. 3, pp. 489–497, June 2011.

[109] S. Villwock, A. Baumuller, M. Pacas, F.-R. Gotz, B. Liu, and V. Barinberg, "Influence of the power density spectrum of the excitation signal on the identification of drives," in *IEEE IECON Conf.*, Orlando, FL, Nov. 2008, pp. 1252–1257.

[110] R. Dhaouadi and K. Kubo, "Transfer function and parameters identification of a motor drive system using adaptive filtering," in *International Workshop on Advanced Motion Control*, vol. 2, Mar. 1996, pp. 588–593.

[111] I. D. Landau and G. Zito, *Digital Control Systems: Design, Identification and Implementation*, 1st ed. Germany: Springer, 2006.

[112] I. Eker and M. Vural, "Experimental online identification of a three-mass mechanical system," in *IEEE CCA Conf.*, vol. 1, Istanbul, Turkey, Jun. 2003, pp. 60–65.

[113] U. Forssell and L. Ljung, "Closed-loop identification revisited," *Automatica*, vol. 35, no. 7, pp. 1215–1241, Jul. 1999.

[114] C. Kaddissi, J.-P. Kenné, and M. Saad, "Identification and real-time control of an electrohydraulic servo system based on nonlinear backstepping," *IEEE/ASME Trans. Mechatronics*, vol. 12, no. 1, pp. 12–22, Feb. 2007.

[115] S. Villwock and M. Pacas, "Time-domain identification method for detecting mechanical backlash in electrical drives," *IEEE Trans. Ind. Electron.*, vol. 56, no. 2, pp. 568–573, Feb. 2009.

[116] L. Bascetta, P. Rocco, and G. Magnani, "Force ripple compensation in linear motors based on closed-loop position-dependent identification," *IEEE/ASME Trans. Mechatronics*, vol. 15, no. 3, pp. 349–359, June 2010.

[117] A. Ghaffari and E. Mohammadiasl, "Calculating the frequency oscillation for servo axes distressed by clearence or preloading," *IEEE/ASME Trans. Mechatronics*, vol. 18, no. 3, pp. 922–931, June 2013.

[118] L. Ljung, *System Identification Toolbox: User's Guide*. Natick, MA: Mathworks, 2010.

[119] L. Peretti and V. Särkimäki, "Mechanical drive train emulation by means of electrical drives - a generalised approach," in *Proc. IEEE IECON '12*, Montreal, QC, Canada, Oct 2012, pp. 1888–1893.

Errata

Publication VI

The denominator polynomials in equation (23) should be $\hat{A}_{\mathrm{d}}(z)(z+\theta_{\mathrm{t}})$ instead of $\hat{A}_{\mathrm{d}}(z)$.

Ac electrical motors supplied with a frequency converter are often selected as torque actuators in modern motion control applications. The mechanical nature of these applications tends to be a resonating one. The mechanical resonances lower the overall accuracy of the system and if the feedback loop is delayed, instability can even occur in the control system. To overcome the resonance problems, this dissertation provides methods to tune stable, robust, and accurate speed-control loop by only using simple classical controllers. The controller tuning relies on the knowledge of the mechanical-system model and its parameters. Thus, this dissertation proposes methods to identify the parameters of the mechanical system.

Aalto-DD 126/2014

ISBN 978-952-60-5826-9
ISBN 978-952-60-5827-6 (pdf)
ISSN-L 1799-4934
ISSN 1799-4934
ISSN 1799-4942 (pdf)

Aalto University
School of Electrical Engineering
Department of Electrical Engineering and Automation
www.aalto.fi